ADVANCED MATERIALS
www.advmat.de

Metal–Drug Coordination Nanoparticles and Hydrogels for Enhanced Delivery

Ka-Ying Wong, Zhenyu Nie, Man-Sau Wong, Yang Wang, and Juewen Liu**

Drug delivery is a key component of nanomedicine, and conventional delivery relies on the adsorption or encapsulation of drug molecules to a nanomaterial. Many delivery vehicles contain metal ions, such as metal–organic frameworks, metal oxides, transition metal dichalcogenides, MXene, and noble metal nanoparticles. These materials have a high metal content and pose potential long-term toxicity concerns leading to difficulties for clinical approval. In this review, recent developments are summarized in the use of drug molecules as ligands for metal coordination forming various nanomaterials and soft materials. In these cases, the drug-to-metal ratio is much higher than conventional adsorption-based strategies. The drug molecules are divided into small-molecule drugs, nucleic acids, and proteins. The formed hybrid materials mainly include nanoparticles and hydrogels, upon which targeting ligands can be grafted to improve efficacy and further decrease toxicity. The application of these materials for addressing cancer, viral infection, bacterial infection inflammatory bowel disease, and bone diseases is reviewed. In the end, some future directions are discussed from fundamental research, materials science, and medicine.

1. Introduction

To enhance the efficacy of drugs and reduce toxicity, formulation plays a significant role within the pharmaceutical industry. Some well-known examples include the encapsulation of doxorubicin (Dox) in PEGylated liposomes to achieve passive tumor targeting.[1] Recently, using lipid nanoparticles (NPs) to deliver mRNA vaccine has spurred a new direction in nanomedicine.[2] Nanomaterials allow for a high loading capacity and also for the conjugation of targeting ligands.[3] While most academic studies have concentrated on the delivery of drugs using inorganic NPs, some of these particles have poor degradability and toxicity. This is due to possible interference with cellular homeostasis, leading to genotoxic effects, oxidative stress, and inflammation in various organs.[4] So far, only a few inorganic materials have been approved,[5] such as ferumoxytol, an iron oxide NP approved in 2009 for the treatment of iron deficiency;[6] and calcium phosphate approved in 1996 to repair craniofacial defects in humans.[7] To solve these problems, smaller-sized inorganic nanocarriers have been engineered to be readily metabolized out of the body.[8] Some metal coordination materials, such as metal–organic frameworks (MOFs) also offer possibilities in efficient drug delivery, sustained release, and synergistic therapy without

K.-Y. Wong, J. Liu
Department of Chemistry
Waterloo Institute for Nanotechnology
University of Waterloo
Waterloo, ON N2L 3G1, Canada
E-mail: liujw@uwaterloo.ca

K.-Y. Wong, M.-S. Wong, J. Liu
Centre for Eye and Vision Research (CEVR)
17W, Hong Kong Science Park, Pak Shek Kok 999077, Hong Kong

Z. Nie
Department of Urology
Xiangya Hospital
Central South University
Changsha 410008, China

Z. Nie, Y. Wang
Institute of Integrative Medicine
Department of Integrated Traditional Chinese and Western Medicine
Xiangya Hospital
Central South University
Changsha 410008, P. R. China
E-mail: wangyang_xy87@csu.edu.cn

M.-S. Wong
Department of Food Science and Nutrition
The Hong Kong Polytechnic University
Hung Hom, Kowloon 999077, Hong Kong

M.-S. Wong
Research Center for Chinese Medicine Innovation
The Hong Kong Polytechnic University
Hung Hom, Kowloon 999077, Hong Kong

Y. Wang
Center for Interdisciplinary Research in Traditional Chinese Medicine
Xiangya Hospital
Central South University
Changsha 410008, P. R. China

The ORCID identification number(s) for the author(s) of this article can be found under https://doi.org/10.1002/adma.202404053

DOI: 10.1002/adma.202404053

significant biological toxicity.[9] Nevertheless, these strategies relied on drug adsorption and still contain high metal content in the drug carrier. Thus, alternative drug delivery systems with a low metal content are desirable.

It has long been noticed that some biomolecules, such as nucleotides and amino acids can form coordination materials with metal ions.[10] For example, an L-aspartic acid (**Figure 1A**) based zirconium-MOF exhibits good chemical stability and proton conduction. This is attributed to the presence of two carboxyl groups with an optimized separation distance, facilitating energetically favorable and robust bridging/linkage of inorganic nodes within the MOF structure.[11] While these ligands are not drugs, these works showed the feasibility of forming drug–metal coordination materials.

Many drugs are rich in metal coordination groups such as amino, carboxyl, and heterocyclic oxygen and nitrogen (Figure 1B–K). They can also form coordination materials with various metal ions yielding NPs and hydrogels. These drug-coordinated materials have a high drug content (and thus low metal content) and the association between drugs and metal ions is through reversible coordination interactions that can be disrupted inside cells or disease microenvironment allowing the release of drugs. On the surface of NPs, targeting ligands can be decorated to home to specific disease sites. In addition, the use of biocompatible metal ions, such as Fe^{2+}, Ca^{2+}, and Zn^{2+} (Figure 1L) are of less safety concerns. Since metals are used to coordinate with drugs, the metal-to-drug ratio is likely to be much lower compared to loading drugs into nanomaterials such as MOFs and porous metal oxides. We will quantitatively illustrate this point in this review.

In this article, we review drug-coordinated materials for therapeutic applications. The types of drugs include small molecules, nucleic acids, and proteins. Although some metal complexes, such as cisplatin, auranofin, and pentostam, have been approved as drugs,[12] and many other metal complexes are in clinical trials or under research, these compounds are outside the scope of this review. This topic has already been extensively reviewed in the medicinal chemistry literature.[13] In addition, many good reviews have been published on metal–drug complexes, which are still consider to be small molecules instead of materials.[14] Thus, they are also outside the scope of the current review. Some other reviews focus on the formation of materials for drug delivery, however the metal ligands themselves are not drugs.[15] These papers will not be covered here either. This review will focus on metal ions that directly coordinate with drug molecules forming materials, such as NPs and hydrogels.

2. Advantages of Metal–Drug Coordination

Metal ions and organic ligands establish coordination bonds through Lewis acid/base interactions, which can occur at room temperature in physiological environments.[16] When a ligand directly donates a pair of electrons to an empty orbital of a metal ion, this is called inner-sphere coordination, which is typically a strong bond. Sometimes, ligand binding occurs via metal-coordinated water or other indirect interactions. This is known as outer-sphere coordination and hydrogen bonding in metal coordination is a typical example of such interactions.

Since the strength of coordination bonds lies between weak intermolecular forces and strong covalent bonds, most metal ligands exhibit good dynamic stability in complex environments.[17] Some coordination complexes are strong enough to survive the circulatory system and can respond to signals of lesion location and accumulate.[18] In addition, various metal ions provide a wide range of unique physicochemical properties and biological functions. Different metal ions exhibit distinct properties in size, binding force, coordination number, direction of bonding, and charge density. These characteristics are utilized to drive the self-assembly of different organic ligands into nanomaterials.[19] Moreover, the unique electronic, optical, magnetic, radioactive, and catalytic properties of different metal ions make them suitable for various medical scenarios.[16] Many transition metal ions are essential in the body, such as iron, copper, zinc, whereas some other ions can have therapeutic and imaging effects such as platinum[20] and gadolinium.[21] For example, the remarkable magnetism of Mn^{2+} and Gd^{3+} allowed them to serve as contrast agents in magnetic resonance imaging.[22] Ca^{2+} can be enriched in tumor cells due to an elevated level of protein synthesis in tumors, which requires Ca^{2+} to assist protein folding. Therefore, metal ions could be applied to tumor imaging or drug delivery to target sites.[23] In addition, Fe^{2+} and Cu^{+} can react with the endogenous hydrogen peroxide (H_2O_2) within cells, leading to the generation of reactive oxygen species (ROS) for use in chemodynamic therapy (CDT) for tumor treatment.[24] We discuss below a few advantages relevant to and sometimes even unique to metal–drug coordination materials for drug delivery.

2.1. A Low Metal Content

Metal ions are the smallest chemical crosslinkers to build polymeric structures. Typically, each metal ion can coordinate with six to eight ligands depending on the size of the ligand and ligand arrangement.[25] Depending on the valency of metal ions used and the structure of drug molecules, a certain molar ratio exists between metal ions and drugs for each coordination material. In **Table 1**, we listed the metal content in terms of both molar ratio and weight percentage in metal-coordinated drugs, and each metal can coordinate to up to six drug molecules. As a result, the metal contents were all lower than 20% with the lowest being 2%. For comparison, the metal content in drug adsorption systems is much higher. We listed a few MOFs and 2D materials due to their high surface area. However, even among them, the lowest metal content was 27%.[26] For nonporous materials, such as CeO_2, the metal content reached 63%.[27] The materials included here all contained metals. Some materials, such as graphene oxide and carbon nanotubes, which do not have metals, are excluded from the discussion, but some of their toxicity was attributed to metal contamination during their synthesis.[28]

2.2. Changing the Lipophilicity of Drugs

The characteristics of a drug, encompassing absorption, distribution, metabolism, excretion, and toxicity (ADMET), are profoundly shaped by its lipophilicity and solubility.[42] These attributes are not only pivotal during formulation development

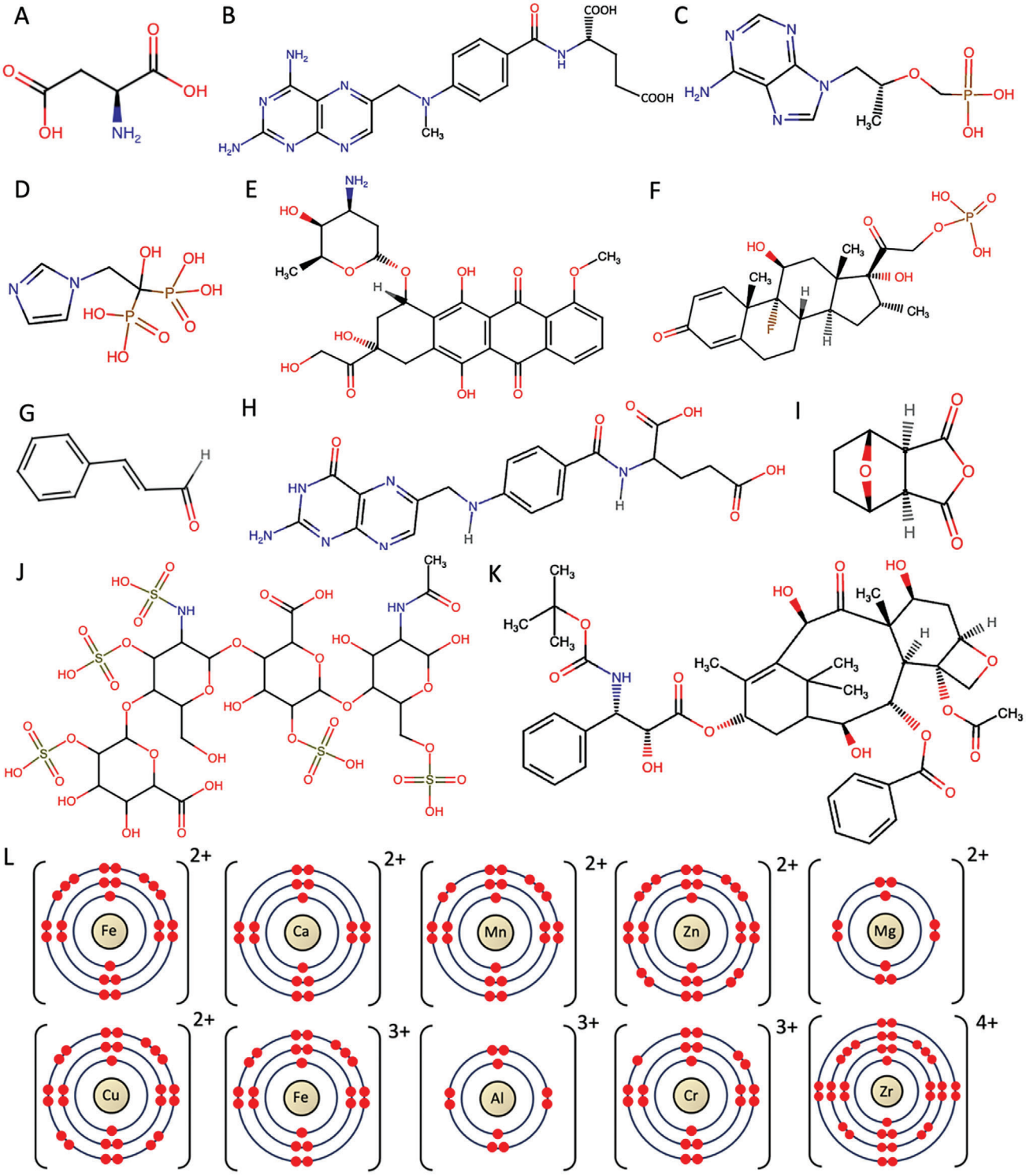

Figure 1. Structural formulas of A) L-aspartic acid, B) methotrexate (MTX), C) tenofovir (TFV), D) zoledronate (ZOL), E) doxorubicin (Dox), F) dexamethasone phosphate (DexP), G) cinnamaldehyde (CA), H) folic acid (FA), I) norcantharidin (NCTD), J) heparin (HEP), K) docetaxel (DXT), and L) A few metal ions used to form coordination materials with drugs.

Table 1. Examples of different metal–drug formulation in molar ratio and metal content.

Drug loading[a)]	Metal	Drug	Form	Metal: drug	Metal [%]	Drug [%]	Release rate	Refs.
Coordination	Fe^{3+}	MTX	NP	1:6	2	98	22% (pH 7.4); 72% (pH 5.0) in 48 h	[29]
	Fe^{3+}	ZOL	NP	1:1[b)]	17[b)]	83	Less than 10% (pH 7.4) in 144 h in PBS	[30]
	Fe^{3+}	Dox	NP	1:1.5[b)]	7[b)]	93	10% (pH 7.0); 77% (pH 5.0) in 60 h	[31]
	Fe^{2+}	Dox	NP	1:1[b)]	10[b)]	90	7% (pH 7.4); 40% (pH 5.0) in 72 h	[32]
	Fe^{2+}	DexP	NP	1:1[b)]	14[b)]	86	N/A	[33]
	$[ZrO]^{2+}$	GAP, TFV	NP	1:2[b)]	16[b)]	84	43% of TFV and 33% of GAP in 24 h in FBS	[34]
	Cu^{2+}	DOX	HG	1:2	5	95	<10% (pH 7.2); 60% (pH 5.0) in 48 h	[35]
	Fe^{3+}	Cat	HG	1:3	14	86	50% (pH 7.4) in 24 h	[36]
	Cu^{2+}	GA	HG	1:2	3	97	85% (pH 7.4); >95% (pH 6.5) in 25 h	[37]
	Ca^{2+}	DexP	HG	1:1.4[b)]	6[b)]	94	>50% in 24 h and the rest in 72 h (pH 7.4)	[38]
	Zn^{2+}	CA and FA	HG	1:0.7	14	86	100% of CA and 76.6% of FA in 72 h in FBS (pH 7.4)	[39]
Adsorption	Zn^{2+}	Dox	ZIF-8 MOF	10:1	23[c)]	16	48.5% (pH 7.4); 68.8% (pH 5.0) in 12 days	[40]
	Mo^{4+}	Dox	MoS_2-nanofibers	24:1	48[c)]	3.7	11.0% (pH 7.4); 65.8% (pH 5.4, 54 °C) in 25 h in PBS	[41]
	Ti^{4+}	Dox	MXene ($Ti_3C_2T_x$) nanosheets	1:1	23[c)]	73	4.8% (pH 7.4); 8.2% (pH 5.5) in 24 h	[26]
	Ce^{4+}	Dox	CeO_2 NP	10:1	63[c)]	22	6.2 (pH 7.4) in 48 h in PBS	[27]

[a)] Abbreviation: HG: Hydrogels; 4-VP: 4-vinyl pyridine; CA: Cinnamaldehyde; Cat: Catechol; DexP: Dexamethasone phosphate; Dox: Doxorubicin; DXT: Docetaxel; FA: Folic acid; GA: Glycyrrhizic acid; NCTD: Norcantharidin; NP: Nanoparticle; N/A: Not available; MOF: Metal–organic framework; MTX: Methotrexate; ZOL: Zoledronate; [b)] The authors did not delineate the metal-to-drug ratio in the publications. This ratio was derived through calculation, leveraging the respective charges of the metal and drug for coordination. Furthermore, the quantification of the metal percentage was predicated upon the molar ratio. For example, in Dox-Fe, where Fe^{3+} has 3 positive charges and Dox has 2 negative charges, we assume that one metal ion could coordinate with two drug molecules, resulting in a molar ratio of 1:1.5. The metal percentage was calculated by dividing the molecular weight of Fe^{3+} by the molecular weight of Dox-Fe, and then multiplying by 100%; [c)] The determination of the metal% was calculated by subtracting the reported drug loading content and nonmetal component from 100%.

but also have considerable influences on the drug's behavior within the body. The 1-octanol/water partition coefficient (*P*) is a widely accepted metric for gauging lipophilicity, holding particular importance in estimating drug behavior. For drugs designed to target the central nervous system, attaining an optimal log*P* value of ≈2 is deemed advantageous for facilitating passive penetration through the blood–brain barrier (BBB).[42,43] Many drugs exhibit high hydrophobicity, posing challenges to absorption and limiting their applicability and chance of success in clinical trials.[44] To address this, nanomedicine formulations, such as liposomes, emulsions, and microemulsions have been explored.[44] These formulations effectively reduce drug particle size from micro- to nanolevel, consequently increasing the surface-area-to-volume ratio.[45] This enhancement in surface area contributes to improved dissolution rates and drug absorption in the body, thereby augmenting the overall bioavailability for drugs.[46] Another strategy involves altering drug properties by forming metal complexes.[42]

Understanding and manipulating these factors contribute to the refinement of drug properties, enhancing their overall therapeutic efficacy. For instance, M'bitsi-Ibouily et al.[47] synthesized a complex involving Ru^{2+} coordinated with antipsychotic sulpiride and amino alcohols in equal proportions. This complex demonstrates several advantageous characteristics which includes increasing the solubility of sulpiride in water, slowing down the release of the drug from the metal, enhancing the absorption of the complexed drug through the pig's intestine, and exhibiting low toxicity of the metal complexes. These findings highlight the potential of metal coordination as a safe method for enhancing drug delivery. Additionally, apart from enhancing water solubility, it has been documented that increasing the lipophilicity of drugs through metal coordination could also enhance drug delivery. For instance, satraplatin, known chemically as bis-(acetate)-ammine dichloro-(cyclohexylamine) platinum(IV), primarily enters tumor cells through passive diffusion, likely due to its enhanced lipophilicity.[48]

2.3. Responding to Disease Microenvironment

Metal coordination provides a unique way to develop drug formulations that can respond to disease microenvironment. The current treatment of tumors has transitioned from targeting tumor cells to treating the tumor microenvironment (TME). The TME is where tumor cells grow and is typically composed of tumor cells, immune and inflammatory cells, tumor-associated fibroblasts, blood vessels, extracellular matrix, and various cytokines.[49] The metabolic activity of tumors affects the changes in the TME, and the TME can in turn influence the growth, proliferation, invasion, metastasis, or apoptosis. Vascular abnormalities and hypoxia are the most common features in the TME.[50] Blood vessels in the TME are usually composed of the disorderly arrangement of defective endothelial cells, which have higher permeability.[51] Given this, NPs with sizes in the range of 20–200 nm are inclined to infiltrate the intercellular space.[52] Coordinated drugs can be synthesized in this size range to enhance accumulation in tumors.

The rapid proliferation state and tissue structure of tumor cells limit the diffusion effect of oxygen.[53] The local oxygen partial pressure may even approach 0 mm Hg in some solid tumors, whereas it is ≈30 mm Hg in normal tissues.[54] Hypoxia can directly lead to an acidic microenvironment as tumor cells produce a large amount of lactate when affected by hypoxia.[55] Using Fe^{2+} or Cu^{2+}, which can promote the Fenton reaction, to induce the generation of ROS in the TME is a feasible approach.[56] In addition, an acidic environment can facilitate the dissociation of metal coordination interactions because protons can compete with metal ions for drug binding. Other biological molecules such as ATP and GSH are also strong metal ligands, and they prefer to coordinate with hard/intermediate and soft metal ions, respectively, which may compete for metal coordination to facilitate drug release.[20,57] The cytosol of cancer cells contains 1–10 mM ATP, while the extracellular space contains less than 0.4 mM ATP. This concentration gradient can be harness for ATP-responsive drug delivery.[58]

Aside from tumors, other diseases also have their unique microenvironment. For example, diabetic patients have a risk of community-acquired bacterial infections, like streptococcal infection, due to a high glucose level.[59] Tang et al.[60] developed a bi-functional hybrid nanoflower to combat bacterial infections in response to glucose. This nanoflower incorporated Cu^{2+} coordination with guanosine monophosphate (GMP) and glucose oxidase (GOx). GOx facilitates a glucose-powered cascade catalytic reaction, converting glucose to H_2O_2 and gluconic acid, creating an optimal pH environment conducive to CDT. Consequently, ROS are generated in situ, effectively targeting and killing bacteria. Additionally, Nan et al.[61] engineered a pressure-sensitive acrylic adhesive to regulate transdermal drug delivery. They incorporated ketoprofen and donepezil as model drugs, along with N-[tris(hydroxymethyl)methyl] acrylamide (NAT) coordinated with Fe^{3+}. Fe^{3+} coordination effectively minimized the burst release of the drug from the patches. Furthermore, the coordination interaction between ketoprofen and Fe^{3+} controlled the release of ketoprofen. Taken together, by remaining inactive under normal conditions and activating in response to changes, such as redox status, pH, or light exposure, this controlled activation minimizes side effects by deactivating the drug until it reaches its target.[20]

2.4. Other Advantages of Metal Coordination

Metal–drug coordination materials can demonstrate synergistic therapeutic effects. For instance, metal ions can produce Fenton reactions to enhance the toxicity of its coordinated drugs.[29] In addition, metal–drug coordination may lower drug toxicity. This is attributed to the formation of coordination bonds between the drug and metal, which enhances the stability of drugs in the bloodstream and reduces toxicity.[34] Finally, metal coordination offers porous structures suitable for encapsulating other drug molecules, facilitating a controlled release mechanism.[62]

3. Types of Materials Formed by Metal–Drug Coordination

Metal coordination can make many types of materials, and a popular one is MOF. MOFs are porous crystalline materials, and they are very popular for drug loading. For example, Liu et al.[63] developed multifunctional hydrogel eye drops (named DCFH) for the synergistic treatment of uveitis by mixing dexamethasone (Dex) as the anti-inflammatory agent and the active oxygen scavenger cerium-based metal organic framework (Ce-MOFs) into a thermosensitive triblock copolymer F127. Similarly, Tian et al.[64] designed a copper-based MOF loaded with sorafenib in response to GSH for the treatment of hepatocellular carcinoma. These copper-based MOFs can also make tumors sensitive to ferroptosis by releasing Cu^{2+} locally to the tumor. In addition, metal coordination can also form fibers, amorphous nanoparticles, and hydrogels.

Drug molecules often have a large and asymmetric structure, and this has limited the type of material that can be formed. For example, we cannot find any instances of MOFs formed by metal–drug coordination. When biomacromolecule-based drugs, such as proteins and nucleic acids are used, the chance of forming crystalline materials is even smaller. Based on the literature search, we could only find examples of NPs and hydrogels formed by metal–drug coordination. Therefore, the rest of this review is devoted to these two types of materials. For each type, the drugs will be categorized into small molecules, nucleic acids, and proteins.

4. Metal–Drug Coordination NPs

NPs have a small size suitable for both systemic and local delivery. Metal–drug coordination NPs have been explored as a promising platform to deliver drugs, particularly in cancer management. They offer strengths such as augmented stability, prolonged drug half-in blood circulation, and enhanced distribution to target site.[65]

4.1. Small Molecule Drugs

This section is organized based on different types of small molecule drugs that are metal ligands. Small molecules refer to drugs with a molecular weight below 1000 Da.

4.1.1. Pteridines

Tu et al.[29] developed a metal-coordinated NP for synergistic photo-chemotherapy. They coassembled a photosensitizer indocyanine green (ICG) and a chemo-drug methotrexate (MTX, a member of pteridines, Figure 1B) by coordinating negatively charged MTX with positively charged Fe^{3+} by mixing them in an organic solvent, resulting in ICG-MTX-Fe^{3+} NPs with a 94% drug encapsulation efficiency and a NP size of 4 nm. In HeLa cells and HeLa tumor-bearing nude mice, ICG-MTX-Fe^{3+} plus laser treatment showed the most significant photo-chemotherapeutic effect, reducing the tumor size and causing cell death, compared to all the controls. Notably, ICG alone demonstrated poor photostability due to the saturation of double bonds on its conjugate chains, making it less favorable for phototherapy. However, ICG-MTX-Fe^{3+} has good photostability making it suitable for photochemotherapy.

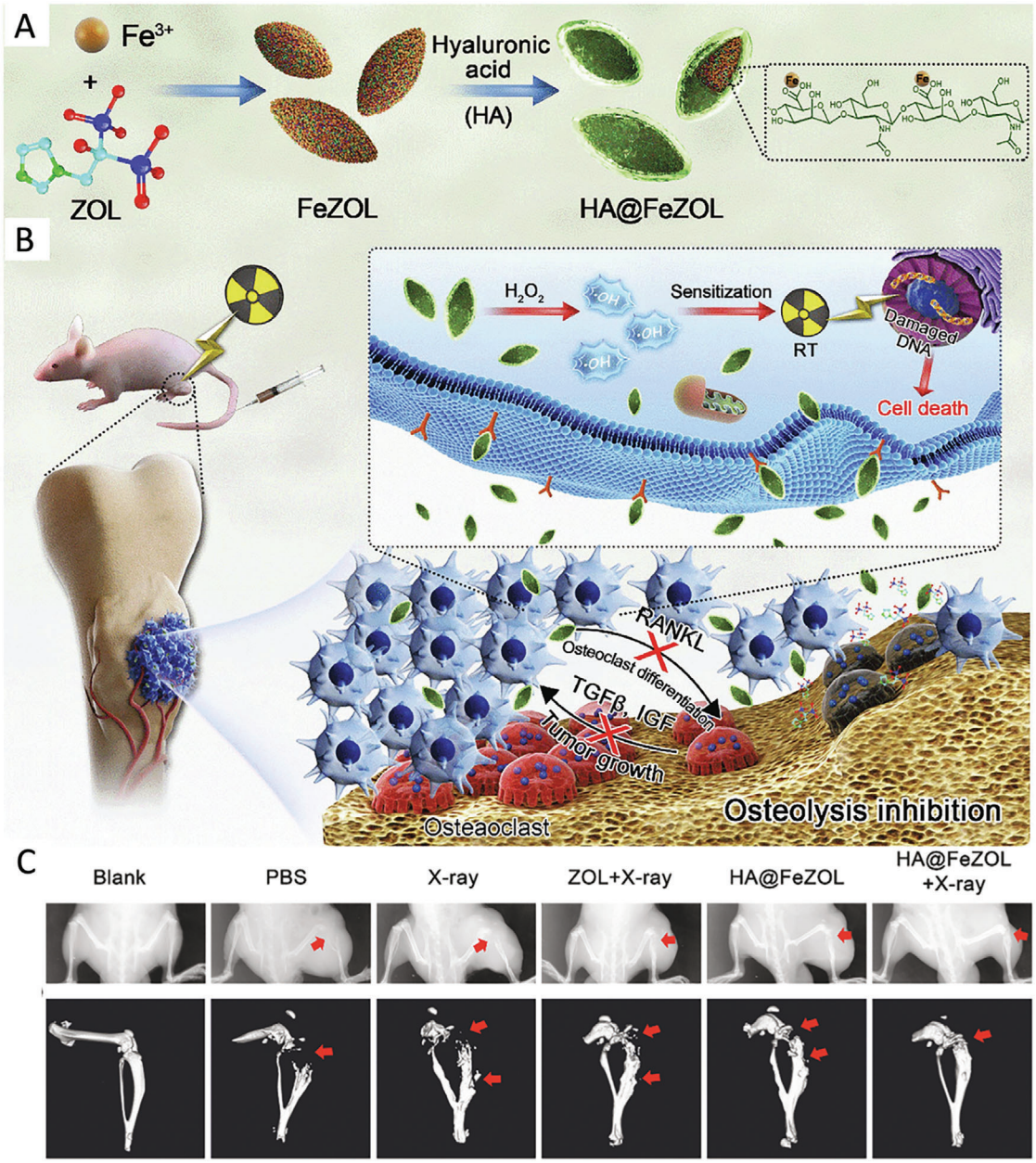

Figure 2. A) Representation of the synthesis of the HA@FeZOL NPs. B) Depiction of the approach to address osteosarcoma through the incorporation of radiotherapy sensitization and suppression of osteoclastogenesis. C) X-ray radiography of mice received different treatments 1 day before sacrifice, with soft tissue contours indicating tumors, and arrows highlighting osteolytic lesions. Adapted with permission.[30] Copyright 2021, Elsevier.

4.1.2. Bisphosphonates

In addition to the direct metal coordination with small molecules, an alternative modality involves the coating of metal-coordinated NPs with a biomimetic membrane or onto other materials to optimize delivery efficacy. Geng et al.[30] introduced core–shell metal–drug NPs based on Fe^{3+}-Zoledronate (ZOL, a bisphosphonate Figure 1D) for treating osteosarcoma, combining radiotherapy sensitization and osteolysis inhibition. The core, formed through the self-assembly of Fe^{3+} with ZOL, was modified with hyaluronic acid (HA) to enhance the targeting effect toward cancer cells with CD44 overexpression (**Figure 2A**). The resulting hybrid HA@FeZOL NPs armed with intrinsic ZOL and HA surface modifications facilitated the evasion of skeletal absorption and ZOL accumulation at osteosarcoma. Upon accumulation, the released ZOL actively reduced osteoclastogenesis in the surroundings, preventing osteolysis. Simultaneously, HA@FeZOL generated free radicals via a Fenton-like reaction amplified radiotherapy, leading to tumor cell death (Figure 2B). Among different treatments, HA@FeZOL plus X-ray exhibited the most potent therapeutic effects in terms of osteolytic lesions and osteoclastogenesis (Figure 2C). The fluorescence intensity of

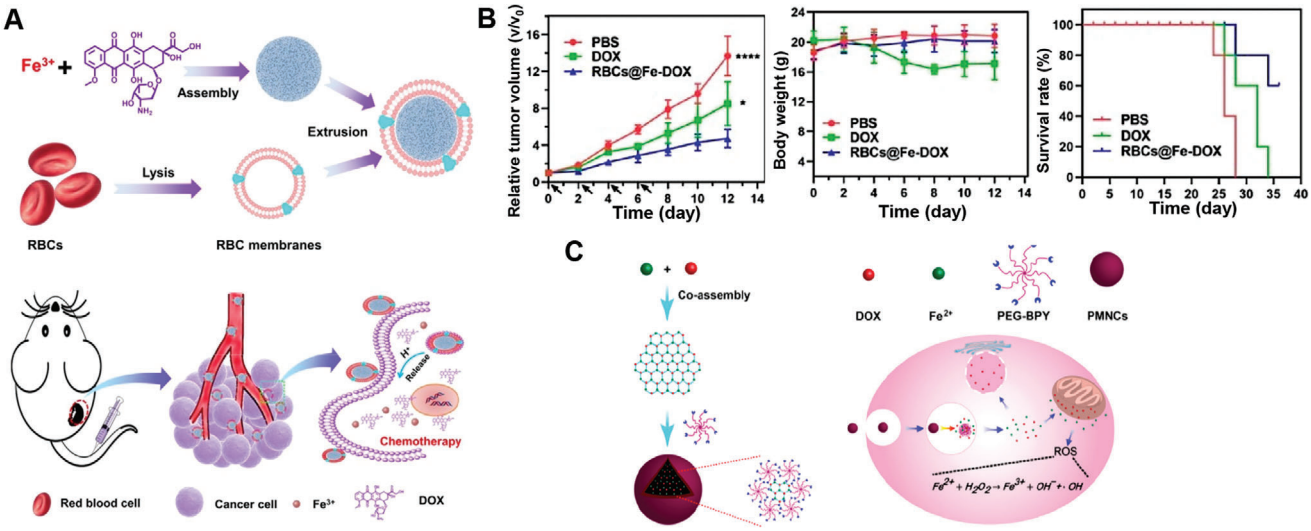

Figure 3. A) A scheme showing the preparation and action mechanism of RBCs@Fe-Dox MDNs for chemotherapy. B) The tumor growth curves, body weight and survival rate of mice after treatment with PBS, Dox, and RBCs@Fe-Dox. Adapted with permission.[31] Copyright 2021, Europen Chemical Societies Publishing. C) A scheme showing the formation of PMNCs for cancer therapy in a synergistic manner. Adapted with permission.[32] Copyright 2019, American Chemical Society.

HA@FeZOL-Cy7.5 in the tumor steadily increased over time, surpassing that of ZOL-Cy7.5 at 1, 6, and 24 h postintravenous injection in orthotopic osteosarcoma mice.[30] This study showcased the promising therapeutic impact of surface modification of metal-coordinated NPs in terms of retention time and anticancer activity.

4.1.3. Anthracycline

Liang et al.[31] synthesized metal–drug coordination NPs through the self-assembly of Fe^{3+} ions and Dox, a anthracycline drug (Figure 1E) for melanoma treatment. The resulting NPs, characterized by a diameter of 82 nm, underwent subsequent coating with red blood cell (RBC) membranes (RBCs@Fe-Dox) through extraction, imparting commendable biocompatibility and an extended circulation lifetime (**Figure 3A**). The utilization of a membrane coating, designed to maintain the structural integrity and antigenic profile of the source cells, led to low intrinsic immunogenicity.[66] This feature enhanced the potential of these systems for drug delivery across various therapeutic applications. In contrast to the passive diffusion of Dox through cancer cell membranes, the coated NPs could be internalized in the cells through endocytosis. This mechanism facilitated a gradual release of conjugated Dox, leading to promoted antitumor effects in compression to free Dox in the context of B16 tumor-bearing mice (Figure 3B,C). However, this study would be more convincing with the inclusion of a control group with uncoated Fe-Dox to show the necessity of the RBC membrane.

In addition to membrane coating, Ruan et al.[32] designed a NPs formulation that enables the intracellular co-delivery of Fe^{2+} and Dox with surface decoration. The process involved the autonomous assembly of Dox and Fe^{2+} through coordination interactions between drug and metal, followed by the surface decoration of multiarmed PEG-dipyridine, enhancing water solubility and stealthy performance. The synthesis included 2,3-bipyridine end-capped eight-armed poly(ethylene glycol) (PEG−BPY) through a carbodiimide (EDC)-mediated amidation reaction between eight-armed PEG−amines and 2,3-bipyridine-6-carboxylic acid (Figure 3C). PEG−BPY and Dox self-assembled into polymer/drug NPs through hydrophobic interactions and $\pi-\pi$ stacking. This NP showed an exceptional drug-loading capability exceeding 40% and favorable kinetic stability. The intracellular release of Dox occurred in a pH-sensitive manner at the tumor site, while the mitochondria-targeted Fe^{2+} overload intensified Fenton-like activity. This process generated ROS within the endosomal acidic pH environment in mouse bladder carcinoma MB49 cells. This method provided a straightforward approach to fabricating metal-coordinated NPs for synergistic therapy. However, this study did not have a free drug control and was limited to in vitro experiments. Further analysis of such NPs in vivo is crucial to explore pharmacokinetics of in the design.

4.1.4. Steroid

Osteoarthritis, a chronic joint disorder associated with inflammation, often relies on intra-articular corticosteroid administration for pain relief and inflammation control. However, challenges arise due to rapid clearance and the necessity for repetitive injections, limiting the efficacy of local anti-inflammatory treatment.[33,67] To address these challenges, Tang et al.[33] devised a metal–drug coordination-driven self-assembly technique for carrier-free delivery of dexamethasone sodium phosphate (DexP, an adrenocortical steroid, Figure 1F) using Fe^{2+}. This approach resulted in the efficient encapsulation of DexP through a one-step assembly with Fe^{2+} by heating at 95 °C for 3 h, producing NPs (Fe-DexP, 113–184 nm) with a drug loading content of

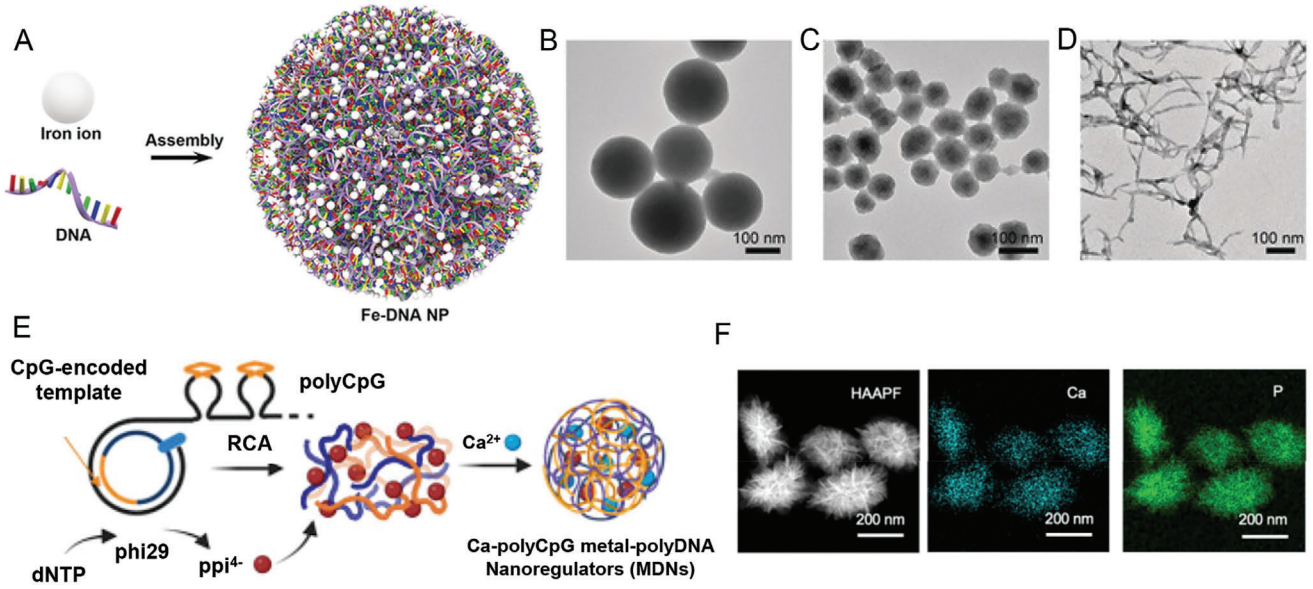

Figure 4. A) A scheme showing coordination-drive formation of Fe^{2+}/DNA NPs. TEM micrographs of NPs formed by Fe^{2+} and B) A20, C) C20, and D) G20 DNA after heating at 95 °C for 3 h. Adapted with permission.[74] Copyright 2019, John Wiley & Sons Inc. E) A scheme showing the preparation of Ca-polyCpG NPs by adding Ca^{2+} to the RCA product containing polyCpG. F) A TEM image and the element mapping of the Ca-polyCpG NPs. Adapted with permission.[81] Copyright 2023, AAAS.

49.3%. With the intra-articular administration of Fe-DexP to an osteoarthritis mouse model, Fe-DexP demonstrated enhanced anti-inflammatory capacity and exhibited gradual degradation within 4 days, ensuring sustained cargo release and mitigated synovial inflammation to hinder cartilage destruction. The degradation of Fe-DexP NPs in the target site was attributed to the weakened Fe-DexP coordination interactions by competitive interactions of phosphate ions. Further studies are warranted to elucidate the feasibility and efficacy of this approach compared to current clinical treatments.

4.1.5. Nucleoside Analogs

Hepatitis B constitutes a significant worldwide disease, and common therapeutic modalities usually have pronounced unexpected and suboptimal effects upon administration into the circulatory system, and persistent long-term inflammation.[34,68] Dong et al. assembled antiviral tenofovir (TFV, Figure 1C) and anti-inflammatory phosphorylated glycyrrhetinic acid (GAP) by coordination with $[ZrO]^{2+}$ relying on ionic interactions.[34] The molar ratio of GAP, TFV, and $[ZrO]^{2+}$ was 1:6:8. This yields a stable NP in serum with a 70% drug-loading capacity and a hydrodynamic diameter of 122 nm for 24 h. Notably, the nanoassembly exhibits prolonged retention in the liver for 72 h, contrasting with nondetectable levels of free TFV 24 h postintravenous injection in murine models. Also, this nanoassembly reduced TFV leakage into the bloodstream and concurrent inflammation mitigation, suggesting a stable and safer administration method for TFV. While the study is clear, further research, especially in detailed pharmacokinetics and biological assays, is needed to establish the efficacy of these NPs in Hepatitis B treatment.

4.2. Nucleic Acid Drugs

Nucleic acids are highly important drugs for gene therapy. For DNA, some representative drugs include cytosine-phosphorothioate-guanine (CpG) oligonucleotides for stimulating the immune system,[69] and antisense DNA and DNAzymes for inhibiting and cleaving mRNA.[70] In addition, DNA aptamers can be used as enzyme inhibitors.[71] For RNA, some representative examples include siRNA for silencing mRNA. Recently, mRNA vaccine has received a lot of attention with the award of the Nobel Prize in 2023. For any nucleic acid-based therapeutic application, delivery is a key obstacle.[72] The field started with condensing nucleic acids with cationic polymers, lipids, and NPs. However, cationic polymeric materials are cytotoxic and safety alternatives are constantly being developed. Metal coordination provides a new route since it completely circumvents cationic polymers and introduces minimal additional materials. Nucleic acids serve as a major component of the resulting nanomaterial for delivery. This section provides a review of some recent examples.

4.2.1. CpG Oligonucleotides

Nucleic acids, such as antisense DNA, siRNA, and more recently mRNA vaccines, can serve as excellent therapeutic agents. Studies have also shown that metal coordination can form NPs with nucleic acids.[73] The Li group first demonstrated that heating Fe^{2+} with single-stranded DNA oligonucleotides at 95 °C for 3 h can produce highly stable coordination NPs (**Figure 4A**).[74] Using A20 and C20 DNA, spherical particles of 213 and 71 nm in diameter were obtained, respectively Figure (4B,C). Over 80% of DNA strands were loaded into these particles. G20 DNA resulted

in nanofibers (Figure 4D), whereas T20 did not produce any hybrid materials. Fe^{2+} is known to replace Mg^{2+} in many nucleic acid structures, but with stronger coordination interactions.[75] This result suggested that DNA bases were involved in binding to Fe^{2+}. In this work, the authors also synthesized Fe–CpG NPs, where CpG oligonucleotides contained unmethylated cytosine–guanine motifs and they can stimulate immune responses of macrophages for cancer therapy.[76] The Fe–CpG NPs could be found in the endosomes or lysosomes of cells. The Fe–CpG NPs enhanced the production of cytokines, suggesting that the DNA in the NPs can be released inside cells. The authors further delivered the NPs to 4T1-breast-tumor-bearing mice and observed a high antitumor activity of Fe–CpG NPs, which was attributed to a high cellular uptake, high loading of CpG, and increased enhanced permeability and retention (EPR) effect.

Using the same heating method, the Song group synthesized an immunostimulator, CpG NPs, with various surface topographies by changing the buffer of synthesis.[77] The authors believed that these Fe^{2+}/CpG NPs could activate the innate immune system biologically and physically. They found that the pompon-shaped NPs demonstrated the best adjuvant properties and antitumor effect in melanoma-bearing mice. The Song group also designed a diblock DNA containing a CpG block and an antisense block, and the DNA was heated to 95 °C with cisplatin to assemble NPs.[78] The authors demonstrated in vitro anticancer effect of the NPs and they further studied the uptake of the NPs by macrophage cells. Under optimal conditions, each cell can load 11.7 ± 1.5 pg of the NPs. In vivo, the authors observed extended circulation in the bloodstream, good tumor homing, and enhanced cancer therapeutic effect.

Ji et al.[79] designed a more sophisticated system by first heating Fe^{2+}, a CpG DNA and metformin (MET) to form NPs. MET serves as an inhibitor for programmed cell death and restores the immune responses of T cells against tumor cells. On this NP, the authors coated a lipid membrane derived from fused tumorous 4T1 cells and RAW264.7 macrophages to present antigens and stimulate effector T cells. Thus, this hybrid NP exhibits a high targeting effect and regulates multiple immune-related processes for antitumor immunotherapy. A similar cell membrane coating of Fe^{2+}/CpG DNA NPs was also reported by Li et al.[80] for treating lung cancer.

Aside from cancer therapy, such NPs were also used for treating other diseases. Liu et al.[81] used rolling circle amplification (RCA) to synthesize very long single-stranded DNA with CpG motifs. Pyrophosphate (PPi) was a by-product, which when mixed with Ca^{2+} can assemble the RCA product to form NPs (Figure 4E). In this case, no heating was required, and the synthesis was carried out at 4 °C over 12 h. Ca^{2+} is known to strongly coordinate with phosphate, which is present in both PPi and in the DNA backbone. The product was a porous NP intended for the treatment of osteoporosis (Figure 4F). In this design, polyCpG DNA was intended to suppress differentiation in bone-breaking cells by stimulating the IL-12 production and release. PPi as an analog of bisphosphonates, an antiresorptive agent, could achieve a targeting effect and increase the retention time of the NPs to the bone. Finally, Ca^{2+} can supplement bone mineralization. The authors demonstrated that the NPs could restore bone condition to almost normal levels in osteoporotic mice and rabbits in 1 month.

4.2.2. Antisense DNA

The immunostimulatory effect of CpG DNA is nonspecific, and this coordination method has also been used for the delivery of specific antisense DNA. G3139 is an 18-mer antisense DNA oligonucleotide that targets the mRNA of antiapoptotic protein Bcl-2. G3139 and Dox, a chemotherapeutic drug, were mixed with Fe^{2+} ions to synthesize coordination NPs via the high-temperature route (**Figure 5A**).[82] Given the similar size and shape of the resulting NPs regardless of Dox, the involvement of Dox in iron coordination might be low and Dox can be considered as a cargo in the NPs. In addition, the authors modified the surface of the NPs with zeolitic imidazolate framework-8 (ZIF-8) metal–organic frameworks. Through this simple synthesis method, the authors were able to precisely adjust the molar ratio of Dox and the antisense DNA from 3.5 to 14.5. The NPs efficiently accumulated the DNA in the tumor (Figure 5B). The transversal relaxivity r_2 of the Dox-containing NPs was 4.8-fold larger than that without Dox. T_2-weighted magnetic resonance images were successfully obtained using tumor-bearing nude mice after the intravenous injection. Also, the NPs showed greater necrosis and apoptotic events than control groups missing Dox or using a nonantisense DNA (Figure 5C). Therefore, the iron metal allowed the NPs to serve as a theranostic system for both MRI imaging and combination treatment.

The Li group grew a Zr^{4+}-based PCN-224 nanoMOF and then assembled an antisense oligonucleotide both without and with Dox using this method.[85] This coordination material allowed integrated chemotherapy, gene therapy, and photodynamic therapy for cancer. In addition, under 640 nm light, cytotoxic singlet oxygen was produced to further facilitate the endosomal escape of the NPs. Aside from using Fe^{2+} to assemble DNA, the group also demonstrated the use of Zr^{4+} and the coassembly of multiple DNA strands, indicating that this is a highly versatile method.[86]

4.2.3. DNAzymes

DNAzymes are DNA-based catalysts and they typically require divalent metal ions for activity.[87] For therapeutic applications, RNA-cleaving DNAzymes are the most often used to cleave viral or tumor RNA.[88] Often, additional transition metal ions are required to achieve high activity of DNAzymes inside cells.[89] Therefore, it is quite reasonable to use metal ions to assemble DNAzymes for both DNAzyme delivery and supplying additional metal ions for activity. The Li group reported the synthesis of Cu^{2+}/DNAzyme NPs using the heating method and further coated the NPs with tannic acid (Figure 5D). The 10–23 DNAzyme was designed to cleave the VEGFR2 mRNA for gene therapy, whereas Cu^{2+} was chosen as a CDT agent to use the endogenous H_2O_2 for producing highly toxic hydroxyl radicals. The resulting NPs were uniform 200 nm in diameter and reached a DNAzyme loading efficiency of 85% (Figure 5E).[83] Using a breast cancer model, the authors demonstrated cleavage of the mRNA by the DNAzyme and observed the accumulation of the NPs in tumors with excellent antitumor effects.

Yu et al.[90] assembled a DNAzyme that targets the p53 gene with Fe^{2+} and they further coated the NPs with dopamine-modified HA. The authors intended to achieve ionizing radiation

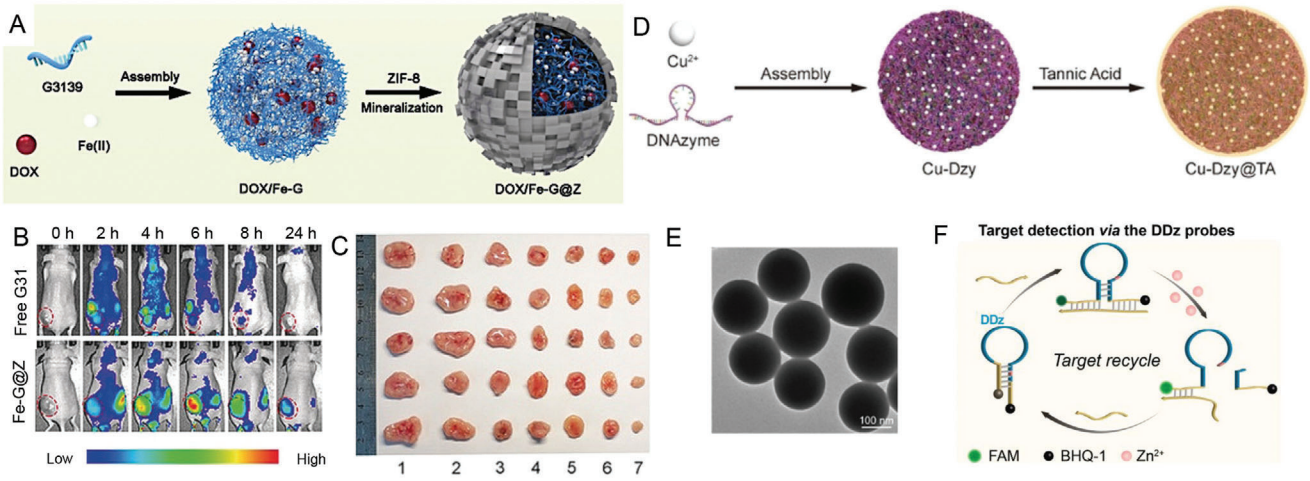

Figure 5. A) A scheme showing co-assembly of an antisense DNA, Dox with Fe^{2+} and further growth of a ZIF-8 layer. B) Fluorescence images showing higher accumulation of G3139 DNA in tumor sites via delivery by the NPs compared to free G3139. C) Tumor photographs of different groups (1: Saline; 2: NPs with nonantisense DNA and without Dox 3: Free G3139 DNA; 4: Free Dox; 5: NPs with antisense DNA; 6: NPs with nonantisense DNA and with Dox; and 7: NPs with antisense and Dox). Adapted with permission.[82] Copyright 2019, John Wiley & Sons Inc. D) Assembly of Cu^{2+} and a DNAzyme and further coating with tannic acid. E) A TEM micrograph of the NPs in (D). Adapted with permission.[83] Copyright 2021 John Wiley & Sons Inc. F) Assembly of a hairpin DNA with Zn^{2+}. Adapted with permission.[84] Copyright 2023, John Wiley & Sons Inc.

to boost ROS levels and amplify Fe^{2+}-mediated ferroptotic damage. The DNAzyme was designed to arrest cells in the G2 phase to enhance the radiation damage. The authors concluded that their hybrid NPs achieved the designed goals to kill tumor cells with radiotherapy with minimal toxic side effects.

A few DNAzyme/Zn^{2+} NPs were reported for sensing applications. We briefly introduce them here since they used a different metal, Zn^{2+}, to achieve the assembly. For example, Zhang et al.[84] mixed a hairpin-structured DNA with a fluorophore and a quencher label with a $Zn(CH_3COO)_2$ solution. The synthesis was performed at room temperature. This hairpin has a DNA-cleaving DNAzyme sequence,[91] that can be activated by the presence of a microRNA (Figure 5F).

Some other therapeutic-related applications include the use of the peroxidase-like nanozyme activity of DNA/Ag^+/Pt^{2+} NPs for antimicrobial applications[92] and the use of DNA/Fe^{2+} with Dox for transdermal delivery.[93]

4.2.4. Therapeutic RNA

RNA has received great attention from the medical community due to its powerful biological therapy capabilities. To date, multiple RNA therapies have been clinically approved for different diseases.[94] mRNA is used to synthesize functional or defective proteins,[95] whereas siRNA is used to reduce the expression of endogenous or pathological proteins.[96] Targeting the delivery of RNA has always been a difficult technical bottleneck due to the quick degradation of exogenous RNA by the body and the blockage to the cell nucleus through the biological membrane system.[97] By contrast, a series of modification measures for RNA have been implemented, such as improving the stability of RNA through chemical modification,[98] enhancing the delivery of specific organs and cells through ligand conjugation,[99] and regulating pharmacokinetics and avoiding escape through nano ion encapsulation of RNA.[100] The unique physical and chemical properties of hydrogels can maintain the biological activity of RNA, retain and continuously release RNA as a local delivery carrier, and release drugs on demand through corresponding stimulation.[101]

This area started with Li's discovery of extended heating DNA and metal mixture to 95 °C. DNA is known to be thermally stable and can survive PCR conditions, easily enduring temperatures as high as 95 °C. RNA, on the other hand, is a much more fragile molecule that is easily degraded even at room temperature. Interestingly, the Yang group heated Zn^{2+} and various RNA and also found NP formation, while still reserving RNA function.[102] Various functional RNAs with lengths ranging from 20 to nearly 1000 nucleotides were successfully tested. For example, the authors used a 996-nucleotide GFP mRNA and a 214-nucleotide circular RNA, and both yielded spherical NPs after reaction with Zn^{2+} (**Figure 6A–D**). Compared to electroporation, the transfection of GFP mRNA showed similar efficacy when delivering GFP mRNA NPs into HeLa cells (Figure 6E–H). The authors further assembled a synthetic single-stranded RNA named AntagomiR-221, which inhibits the upregulation of oncomiR-221, and then wrapped the NPs with red blood cell membranes. This hybrid NP was stable for at least 20 days. This NP showed excellent transfection ability and inhibited the actions of tumorigenic MDA-MB-231 cancer cells.

Liu et al.[103] assembled siRNA using Cu^{2+} for NPs and then coated the NPs with HA for active tumor targeting (Figure 6I). The synthesis was performed at 37 °C for 36 h. The siRNA silenced the catalase gene so that H_2O_2 can be better accumulated in tumor cells. The increased H_2O_2 concentration then can boost the chemdynamic therapy using the Cu^{2+}. Preclinical testing revealed the efficacy of this design. Another siRNA with membrane coating was also reported.[104]

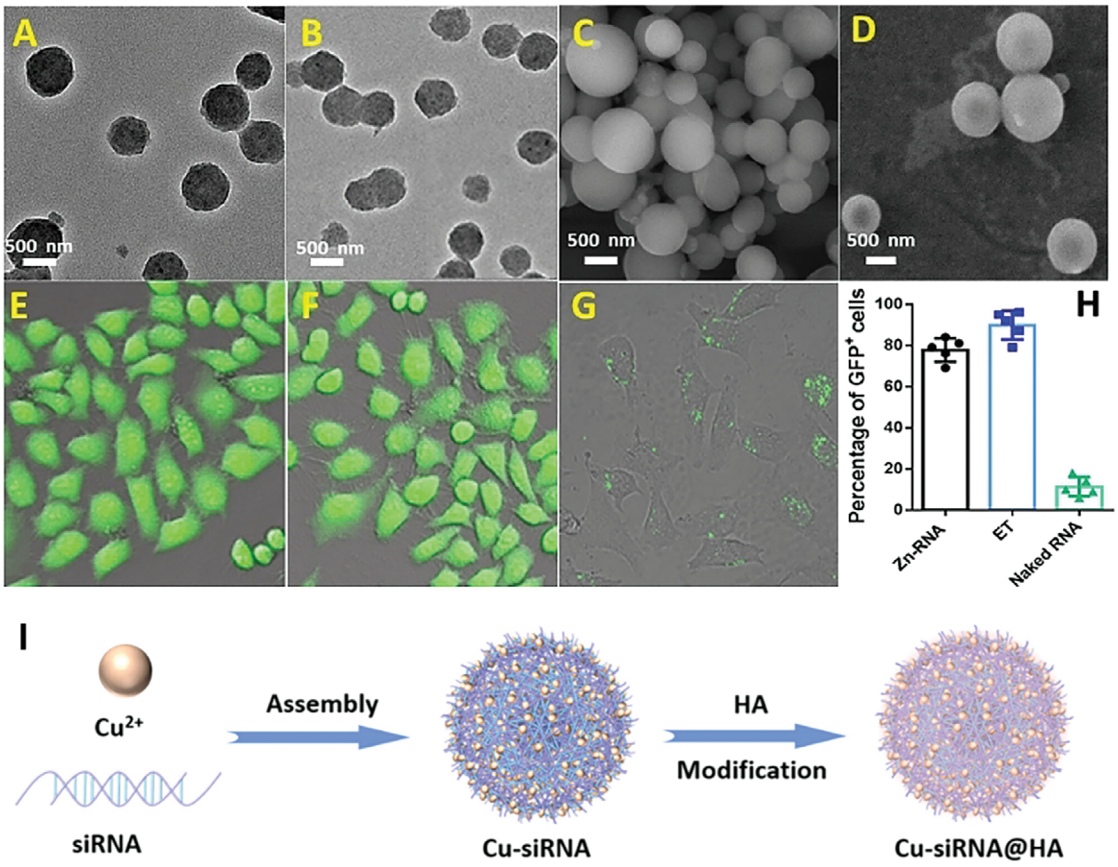

Figure 6. TEM and SEM micrographs of the Zn^{2+}/RNA NPs synthesized using A,C) a 996-nucleotide GFP mRNA, or B,D) a 214-nucleotide circular RNA. Confocal scanning micrographs of HeLa cells transfected with GFP mRNA E) using the Zn^{2+}/RNA NPs, F) electroporation, or F) free GFP mRNA G). H) Comparison of the mRNA delivery efficiency. Adapted with permission.[102] Copyright 2021, John Wiley & Sons Inc. I) A scheme showing the formation of Cu^{2+}/siRNA NPs and coating it with HA. Adapted with permission.[103] Copyright 2023, American Chemical Society.

4.2.5. Fundamental Understanding of Metal Coordination to DNA at High Temperature

Based on the above reviewed literature, there are two types of synthesis methods. One is at high temperature (70–95 °C) and the other at a low temperature between 4 and 37 °C. Usually, a high metal concentration was used at a low temperature. To form NPs, for short DNA, a high DNA concentration is required, and this concentration can be locally high such as when attached to gold NPs.[105] DNA as a polymer has a lower critical solution temperature (LCST) behavior, which is especially obvious for long DNA such as RCA products. LCST refers to the temperature at which hydrophobic interactions start to dominate and DNA condenses to a separate phase. Walther and coworkers studied this using various RCA products and they found that DNA containing a stretch of poly-adenine and poly-guanine are more easily condensed.[106] As shown in **Figure** 7A, adding metal ions such as Mg^{2+} and Ca^{2+} can lower the LCST. Figure 7B shows that a new condensed DNA phase was formed at 70 °C for this sample, whereas the solution was mostly homogeneous at 55 °C. Metal ions like Mg^{2+} and Ca^{2+} do not form very strong interactions with DNA and when the temperature is lowered, the condensed DNA reversibly dissolved to form a homogenous solution again. That's probably the reason that all the above work used transition metal ions, which upon heating may establish strong inner sphere coordination with DNA. We found that Fe^{2+}/DNA NPs formed by heating at 95 °C were extremely stable and even adding EDTA could not dissolve it. Dissolution was observed only when polyphosphate was added as competitor.[107]

While extended heating DNA at close to boiling temperature is expected to degrade DNA, it was found that metal ions can protect DNA from degradation by lowering the lower critical solution temperature (LCST) of DNA and condensing DNA into a thermally stable state.[106b,107] Figure 7C shows that the degradation of a fluorophore-labeled 24-mer DNA was inhibited by Mg^{2+} under the heating condition. When the DNA concentration is lowered by 10-fold, the needed Mg^{2+} concentration to achieve stabilization increased (Figure 7D), which also suggested that stabilization was a result of forming the LSCT-related condensed phase. Aside from using divalent metal ions, Han et al.[108] also used a series of trivalent lanthanide ions to form NPs with DNA by heating at 95 °C.

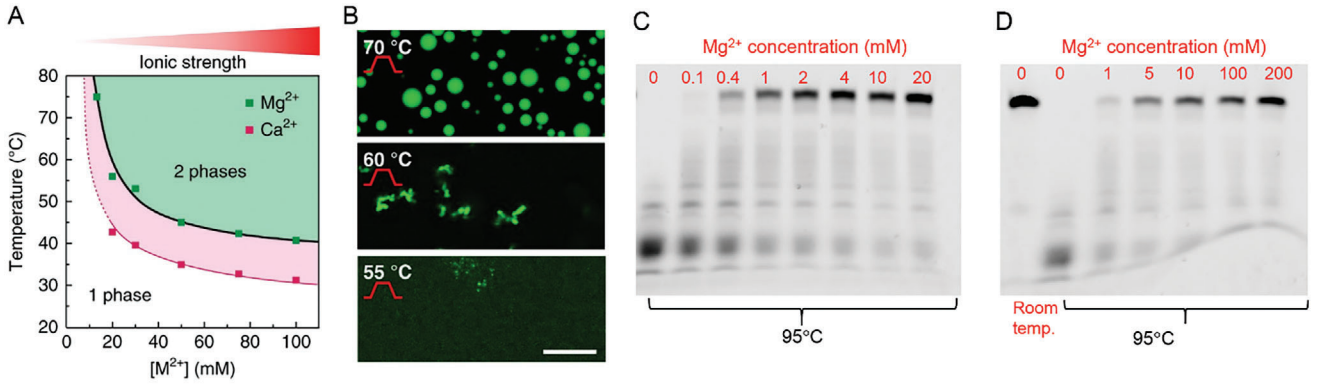

Figure 7. A) The change of the phase separation temperature of 0.06 g L^{-1} of a poly-A-containing RCA product under various concentrations of Mg^{2+} and Ca^{2+}. B) Confocal fluorescence micrograph of the DNA in 50 mM Mg^{2+} after heating for 5 min at 55, 60, and 70 °C and hybridized with a green fluorophore-labeled DNA. Adapted with permission.[106b] Copyright 2018, Nature Publications. Gel micrographs of a FAM-labeled 24-mer DNA after heated at 95 °C for 3 h under various concentrations of Mg^{2+} with a total of C) 4 μM DNA, and D) 0.4 μM DNA. Adapted with permission.[107] Copyright 2022, Royal Society of Chemistry.

4.3. Protein Drugs

Many important drugs are based on peptides and proteins. Almost half of the 50 best-selling pharmaceuticals in 2022 are based on proteins. Some examples include **adalimumab**, pembrolizumab, nivolumab, ocrelizumab, and insulin glargine (**Table 2**).[109] They vary in molecular weight from a few KDa (e.g., insulin glargine) to over 100 KDa for antibodies. Many amino acids possess strong electron-donating groups, allowing them to engage in metal coordination, such as the carboxyl group in glutamic acid, the imidazole group in histidine, and the thiol group in cysteine. The method of metal coordination depends on the selected anchoring sites, aligning with the principles of the hard and soft acid-base theory (**Figure 8A**).[110] While many proteins and peptides are of great therapeutic value, there is limited knowledge regarding NPs composed solely of proteins and metal ions for therapeutic purposes. It might be that proteins are susceptible to denaturation in the presence of a high concentration of transition metal ions.

Delivery of protein drugs to extracellular or intracellular targets poses as a challenge due to their substantial size and chemical properties, rendering them unable to penetrate biological barriers. Additionally, their short half-life in the digestive and circulation systems, along with inherent immunogenicity, further complicates successful delivery.[111] At this moment, it is unclear whether metal coordination can serve as an effective method for forming NPs for the delivery of protein-based drugs. Below, we review a few examples involving proteins and metal ions. However, the following proteins serve only for structural roles.

4.3.1. RNase A

While proteins generally denature irreversibly upon heating, the Li group attempted to assemble RNase A along with an antisense DNA and Fe^{2+} (FeASOR) (Figure 8B).[112] The condition of synthesis was considered slightly mild, with heating maintained was between 75 and 90 °C for 2 h. RNase A is a thermostable protein and Rnases have been used in clinical trials due to their strong RNA cleavage activities to inhibit protein synthesis. A typical molar ratio used for Rnase A: antisense DNA: Fe^{2+} was of 1:2:78. It is unclear whether Rnase A participated in metal coordination

Table 2. Examples of drugs that are based on peptides and proteins.

Drug	Category	Type of protein	MW [KDa]	Disease treated
Insulin glargine	Long-acting insulins	A 52 amino acid protein in an asymmetric unit	5	Diabetes
Dulaglutide	Incretin mimetics	Long-acting glucagon-like peptide 1 analog	59.7	Type 2 diabetes
Aflibercept	Vascular endothelial growth factor-A and placental growth factor antagonists	Recombinant dimeric glycoprotein	96.9	Age-related macular degeneration, macular edema, and diabetic retinopathy
Adalimumab	Tumor necrosis factor inhibitors	Monoclonal antibody	144	Arthritis, ankylosing spondylitis, Crohn's disease, ulcerative colitis
Ocrelizumab	Anti-CD20 monoclonal antibody	Glycosylated cytolytic antibody	145	Relapsing or primary progressive multiple sclerosis
Dupilumab	Interleukin-4 receptor alpha antagonist	Monoclonal antibody	147	Atopic dermatitis, asthma, chronic rhinosinitus with nasal polyps.

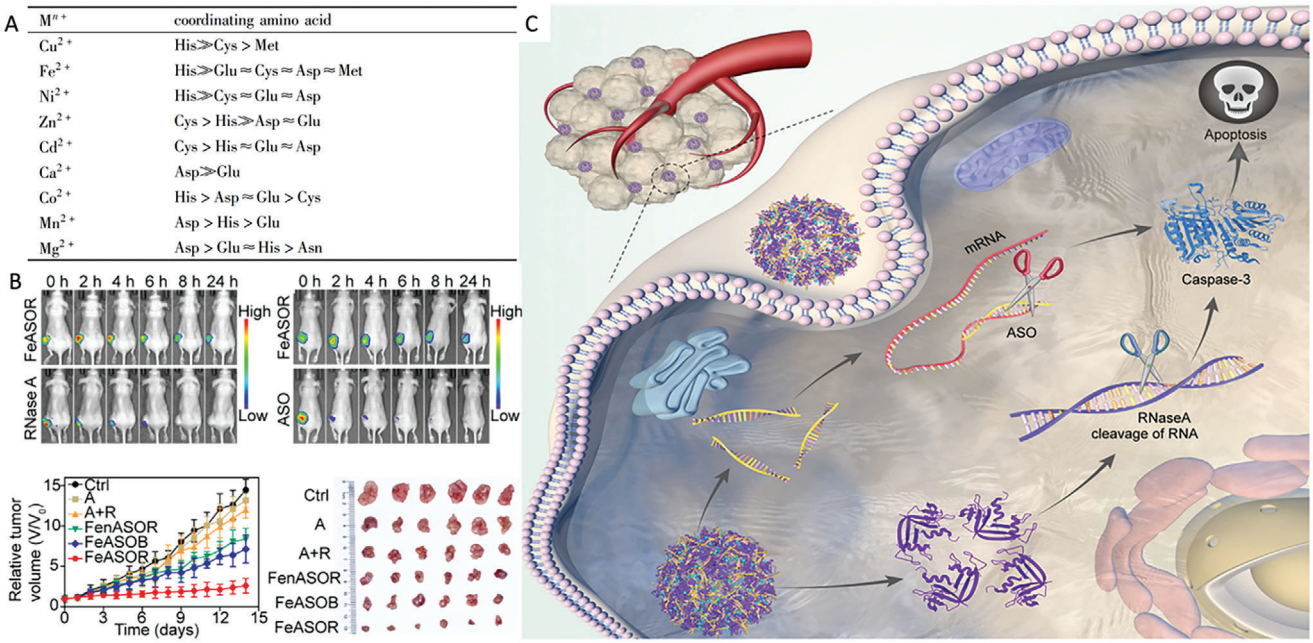

Figure 8. A) Ranking of the occurrence of amino acids coordinated with biological metal ions in the Protein Data Bank. Adapted with permission.[110a] Copyright 2016, Progress in Chemistry. B) A scheme of the coordinated assembly of proteins and nucleic acids within a singular architecture for concurrent delivery to cells and synergistic therapy. C) FeASOR enhances the retention of Rnase A and ASO at tumor sites, leading to a greater reduction in tumor volumes compared to free Rnase A and ASO in a murine model with MCF-7 xenografts. Adapted with permission.[112] Copyright 2021, Elsevier.

or was simply trapped. Based on the ability of histidine and other amino acids to coordinate with iron, it is likely that Rnase A was involved, although the DNA was likely to be the main ligand for iron coordination. The NPs exhibited efficient delivery and demonstrated substantial efficacy in inhibiting tumor growth in a murine model with MCF-7 xenografts. This effectiveness was further highlighted by the prolonged retention time of FeASOR within the tumor, extending up to 24 h postintratumoral administration (Figure 8C). This extended retention stood in contrast to the considerably shorter residence time of 4 h for the administration of Rnase A and antisense DNA as individual agents at the tumor site. This study outlines the self-assembly, carrier-free, and stable codelivery of proteins and DNA using metal coordination for cancer therapy.

4.3.2. Serum Albumin

Supramolecular protein nanodrugs have garnered attention in cancer therapeutics due to its antitumor properties, photothermal efficiency, and low toxicity. However, its stability in the bloodstream is compromised by interactions with abundant blood proteins. To enhance structural stability, Sun et al.[113] designed a protein nanodrug (BPMn NPs, 115 nm) incorporating serum albumin (BSA) and pheophorbide a (PheoA) with Mn^{2+} coordination. In comparison to protein nanodrugs without metal coordination (BP NPs), the addition of Mn^{2+} improved protein and drug content within the NPs, likely attributed to electrostatic interactions, metal coordination, and the metal binding sites of BSA. These BPMn NPs exhibited superior stability when interacting with intracellular molecules, in vivo photothermal conversion and tumor inhibition compared to BP NPs. Surface hydrophobicity of the BPMnH NPs suggests that they have enhanced intermolecular hydrophobic interactions. Additionally, the authors subjected the BPMn NPs to heating (BPMnH NPs) to decrease the surface hydrophobicity of the particles and enhance intermolecular hydrophobic interactions. These modifications could further improve the stability of these NPs.

Argitekin et al.[114] also employed BSA and V^{3+} metal coordination to create pH-responsive dopamine-conjugated BSA-Dox nanoparticles (Dox-D-BSA NPs) for drug delivery. Serum albumin proteins are frequently employed in the production of biocompatible drug nanocarriers because of their ability to efficiently bind both hydrophilic and hydrophobic drugs.[115] Initially, the authors functionalized BSA proteins with catechol-containing dopamine (D) molecules to produce dopamine-conjugated BSA (D-BSA) in the presence of the coupling agent EDC. This conjugation endowed BSA with antioxidant properties. These conjugates were then subjected to reaction with V^{3+} to form 253 nm NPs with metal coordination between BSA and V^{3+}, followed by Dox loading (**Figure 9A**). Dox-D-BSA NPs exhibited superior time-dependent cellular uptake in cancer cells (Figure 9B) and pH-responsive Dox release (Figure 9C). However, further investigations in cancer models are required to compare the efficacy and drug release of Dox-D-BSA NPs with Dox alone to demonstrate the impact of metal coordination NPs. Although BSA is not a drug, these two examples illustrate the feasibility of direct protein-metal coordination for drug delivery. In these two BSA examples, BSA only served structural roles and developing some therapeutic protein-based coordination nanomaterials would be an interesting future direction.

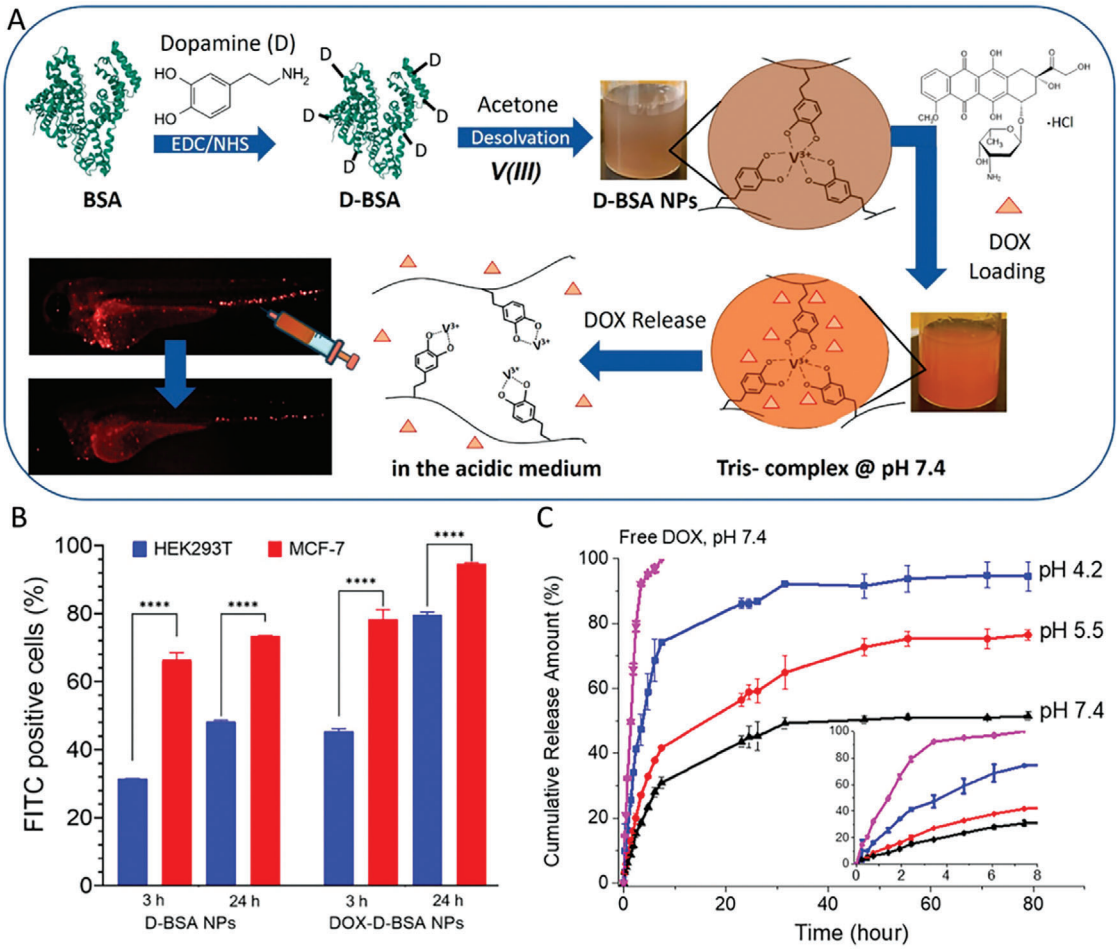

Figure 9. A) Schematic representation of the formation of DOX-D-BSA NPs. At pH 7.4, DOX was incorporated into D-BSA NPs with tris-catechol-V(III) coordination, while release of DOX occurred in an acidic environment through degradation of NPs via formation of mono-catechol-V(III) coordination. Administering DOX-loaded D-BSA NPs into the vasculature of zebrafish larvae effectively eliminated circulating tumor cells. B) The cellular uptake of D-BSA NPs and DOX-D-BSA NPs in HEK293 cells and MCF-7 cells for in 3 and 24 h. C) The pH-responsive release of Dox from DOX-D-BSA NPs. Adapted with permission.[114] Copyright 2023, American Chemical Society.

5. Metal–Drug Coordination Hydrogels

Hydrogels are soft materials consisting of crosslinked polymer chains that swell in water due to their large water content. Such a feature enables it to imitate and fit well to living tissues.[116] Depending on the size, hydrogels can take different forms including NPs, microparticles, and monoliths. While hydrogels can also exist as NPs, hydrogels are a different type of material compared to typical NPs reviewed above due to their high-water content and swelling properties.

The application of hydrogels has already infiltrated our daily life. A typical example is soft contact lenses. This flexible hydrogel material with adjustable optics has led to the establishment of an multibillion dollar industry.[117] Another well-known hydrogel product is the antipyretic patch. Due to a high-water content of hydrogel, it can quickly and effectively reduce the skin surface temperature.[118] If other materials, such as tannic acid or carboxymethyl cellulose are added to the hydrogels, it can be made into a wound dressing with anti-inflammatory, antibacterial, and isolating the surface of the wound from external contact.[119] For example, Zheng et al.[120] designed a multilayered topological hydrogel patch for burn wound first-aid, which can rapidly cool, provide efficient anti-inflammatory effects, and protect wounds. The hydrogel products can also improve the skin permeability and help relax the skin barrier through skin hydration.[121] In addition, hydrogels have been developed for 3D cell culture, cancer treatment, and other fields.[122]

Many external factors regulate the formation and stability of hydrogels, such as pH, temperature, light, redox substances, and organic solvents.[123] The regulation of metal ions in hydrogels has been a powerful method as demonstrated in recent years. For example, hydrogels containing high valent metal ions, such as Zn^{3+}, Hf^{4+}, and Cr^{3+} through coordination bonds usually exhibit excellent water stability.[124] This outcome is attributable to the interaction between metal ions as strong Lewis acids and ligands as strong Lewis bases providing better stability than noncovalent interactions.[125] The strategy of metal coordination hydrogels actually has already been used by nature. This ingenious complex exists in mussel adhesion proteins, enabling them to adhere to various wet surfaces.[126] Several common ligand strategies are

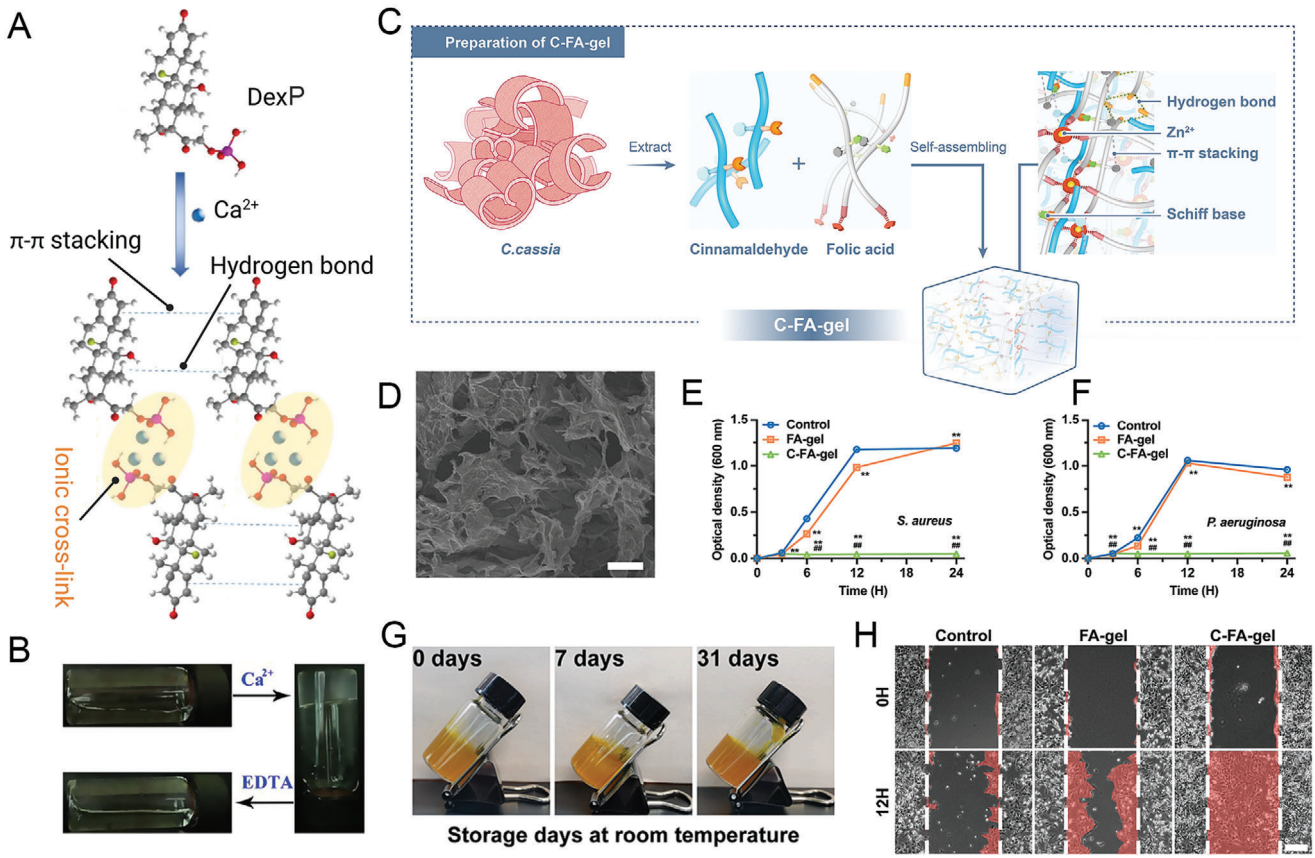

Figure 10. A) Formation of DexP supramolecular hydrogel. B) Photographs of sol–gel–sol transition under the induction of Ca^{2+} and EDTA. Adapted with permission.[38] Copyright 2017, Elsevier. C) The formation of C-FA-gel. D) The images of C-FA-gel were captured by SEM. Scale bar: 40 μm. Growth curves of *Staphylococcus aureus* E) and *Pseudomonas aeruginosa* F) in different formulations, $n = 3$ per group. G) Photos of C-FA-gel kept at various durations at room temperature. H) Representative photos of wound healing experiment for HMECs. Scale bar: 250 μm. Adapted with permission.[39] Copyright 2023, Elsevier.

widely used in the design of hydrogels. For example, hydrogels with metal and catecholamine ligands have good elasticity and self-healing ability.[123b,127] Histidine forms a very stable complex with zinc ions. If the content of histidine in the polypeptide sequence is increased, the toughness of the hydrogel can be improved while maintaining good flexibility and self-healing ability.[128] Bisphosphonates (BPs) are a class of organic phosphorus molecules with a high affinity for Ca^{2+}, making them commonly used as drug carriers for targeting bones. BPs can also chelate various other metal ions, such as Cu^{2+}, Zn^{2+}, and Mg^{2+}.[129] Because each metal ion has a unique charge and affinity in the presence of different ligands, selecting different ions according to unique needs is crucial for obtaining hydrogels with specific properties and functions.[130] For example, some hydrogels composed of Fe^{3+} and Al^{3+} have an extremely fast self-assembly speed (about 1 min) and good antibacterial activity against *Escherichia coli* and *Staphylococcus aureus*.[131] Therefore, based on the arrangement and combination of metal ions and drug, various metal–drug hydrogels with different applications, targets, and biological functions can be designed. This section focuses on these hybrid materials and their related applications.

5.1. Small-Molecule Drugs

According to the molecules that are coordinated to metal ions, medical hydrogels can be divided into three categories: 1) direct hydrogel formation by drug-metal coordination with no other reagents involved; 2) metal-coordination hydrogels for drug loading; and 3) radical polymerization hydrogels.

5.1.1. Direct Hydrogel Formation by Drug–Metal Coordination

Some drugs when mixed with certain metal ions can form hydrogels, suggesting that they formed a coordination polymer structure that swelled in water. DexP is a long-acting steroid hormone and a commonly used drug in the treatment of ophthalmic diseases. It is known for its anti-inflammatory, immunesuppressive, anti-endotoxin, anti-shock, and enhanced stress response properties.[132] DexP has a phosphate group that can bind with hard metal ions. Wu et al.[38] used Ca^{2+} coordination combined with DexP to form an intraocular hydrogel for the treatment of uveitis. After adding EDTA to chelate calcium ions, the liquid state can be restored again (**Figure 10**A,b). The authors

believed that both phosphate-Ca^{2+} coordination and pi–pi stacking between DexP molecules contributed to the gelation. This system greatly extended the retention time of hydrogel and the release time of DexP reached 24 h. Adding more Ca^{2+} slightly reduced the rate of DexP release. The fact that DexP can be released from the gel suggests that the gel is a labile system and Ca^{2+} coordination cannot stably retain the integrity of the gel. It is interesting to note that DexP mixed with Fe^{2+} formed NPs, whereas a hydrogel was formed when mixed with Ca^{2+}. Aside from using different metal ions, the Fe^{2+} coordination was achieved by heating at 95 °C for 3 h, while the Ca^{2+} coordination was achieved by a simple incubation at room temperature.

A variety of therapeutic agents can form multicomponent hydrogels through hydrogen bonding, π–π stacking, metal coordination, hydrophobic and other interactions. This method can provide a strategy for preparing self-assembled hydrogels that cannot be generated by a single component. Another advantage of hydrogel is the availability of injectable hydrogels. Compared with NP drug delivery systems, injectable hydrogels exhibit better delivery efficacy to target sites. For example, Wu et al.[39] used cinnamaldehyde (CA, Figure 1G) and folic acid (FA, Figure 1H) to self-assemble directly into an injectable hydrogel (C–FA gel) through dynamic Schiff base formation and Zn^{2+} coordination as Figure 10C. C-FA-gel had powerful characteristics of shear thinning, injectability, self-healing, and tissue adhesion. In medical applications, C-FA-gel not only had good biocompatibility and nontoxicity but also provided effective time control and sustained drug release at the fitting site. It regulated the microenvironment in the vulnus through various biological activities such as antibacteria, anti-inflammation, and angiogenesis promotion. SEM photos show that the scaffold of hydrogel is a 3D network of lamellar crosslinks (Figure 10D). In the control group, the OD600 values of *Pseudomonas aeruginosa* (Figure 10E) and *Staphylococcus aureus* (Figure 10F) increased significantly within 12 h and reached the peak within 24 h, indicating that these bacteria can rapidly proliferate in the control hydrogel. In the C-FA-gel group, no bacterial colonies were observed, and the OD600 nm value did not increase after more than 24 h. These tests indicate that the antibacterial ability and duration of C-FA-gel are far superior to those of FA-gel. The appearance of the hydrogel is uniformly yellow and has excellent stability, and there is no obvious change in the appearance after 7 and 31 days of storage (Figure 10G). The wound-healing effect could be studied by cell migration. Figure 10H shows that C-FA-gel promotes the healing of human microvascular endothelial cells (HMEC). Compared to the control group, C-FA-gel could be a temporary extracellular matrix to promote the wound healing process involving endothelial cells.

5.1.2. Metal-Coordination Hydrogels for Drug Loading

In another type of hydrogels, metal ions were designed to coordinate with a nondrug polymer while drugs were added at the same time of gelation. It is often unclear whether drug molecules were part of the gel matrix or not. For example, Yavvari et al.[36] designed a self-healing gel using reversible catechol·Fe^{3+} coordination crosslinking. Catechol-modified chitosan was used as the main backbone of the gel and crosslinking was achieved in the presence of Fe^{3+} along with two drugs: hydrophilic Dox and hydrophobic DXT (Figure 1K). The loading of these two drugs was enabled by the amphiphilic nature of the gel. The binary hydrogel of Dox and DXT has a long half-life of 22 days, sustained drug releases over 18 days, and exhibited a good tumor inhibitory effect in vivo.

Hydrogels responding to sound, light, pH, laser, and other signals can also be used to control drug release. Pi et al.[37] used Cu^{2+}-mediated glycyrrhizic acid and norcantharidin (NCTD, Figure 1I) self-assembly for preparing an injectable hydrogel (NCTD gel). When exposed to 808 nm laser irradiation, the gel exhibited ROS and overcome the hypoxia microenvironment to trigger apoptosis and cuproptosis in tumor cells. The CDT effect of the NCTD gel depends on the acidic and elevated level of H_2O_2 in the TME. The targeted controlled release drug of hydrogel can better meet the needs of precision medicine. At the same time, the hydrogel has good biocompatibility, sustainable preparation process, simple and low cost showing great clinical transformation potential in cancer treatment.

Another advantage of hydrogels is that they can be applied locally and directly to the target tissue. For example, contact lens are made of hydrogels and they are a novel platform for drug delivery. An interesting example is that drugs could be slowly released in the eye through the coordination of self-assembled hydrogel through Ca^{2+}/alginate/ DexP. Ca^{2+} with alginate can form hydrogel, and Ca^{2+} with DexP can also form hydrogels. Thus, it is not surprising that a mixture of the three formed a hydrogel as well. The release rate of DexP could be regulated through adjusting Ca^{2+} concentration (**Figure 11A**).[133]

5.1.3. Radical Polymerization Hydrogels with Metal–Drug Coordination

In the final type of hydrogel, the gel matrix was formed via radical polymerization of small molecule monomers, whereas drugs coordinated with metal ions were loaded in the gels. For example, Qing et al.[35] prepared a Dox delivery hydrogel that could respond to pH through coordination with Cu^{2+}. In this system, Dox serves as a template molecule, Cu^{2+} serves as a connecting element for preassembly and 4-vinyl pyridine serves as a functional monomer. Dox and Cu^{2+} were coordinated at a ratio of 2:1. Finally, a hydrogel was prepared using 2-hydroxyethyl methacrylate as the main chain and *N*, *N*-methylenebis acrylamide as the crosslinking agent (Figure 11B). The drug release curve of loaded Dox exhibited a pH-responsive characteristic. At pH 7.2, the release rate of encapsulated Dox occurred at a slow rate, whereas at pH 5.0, the rate significantly accelerated due to the weakened coordination bond between Cu^{2+} and Dox/4-VP.

5.2. Nucleic Acid Drugs

Nucleic-acid-based therapies include promoting the expression of beneficial proteins (such as encoding DNA and mRNA) and silencing malignant gene expression (such as microRNA and siRNA). Many types of nucleic acid drugs were used for treatment, and these polymers have similar physicochemical properties due to the conserved phosphate backbone of nucleic acids.

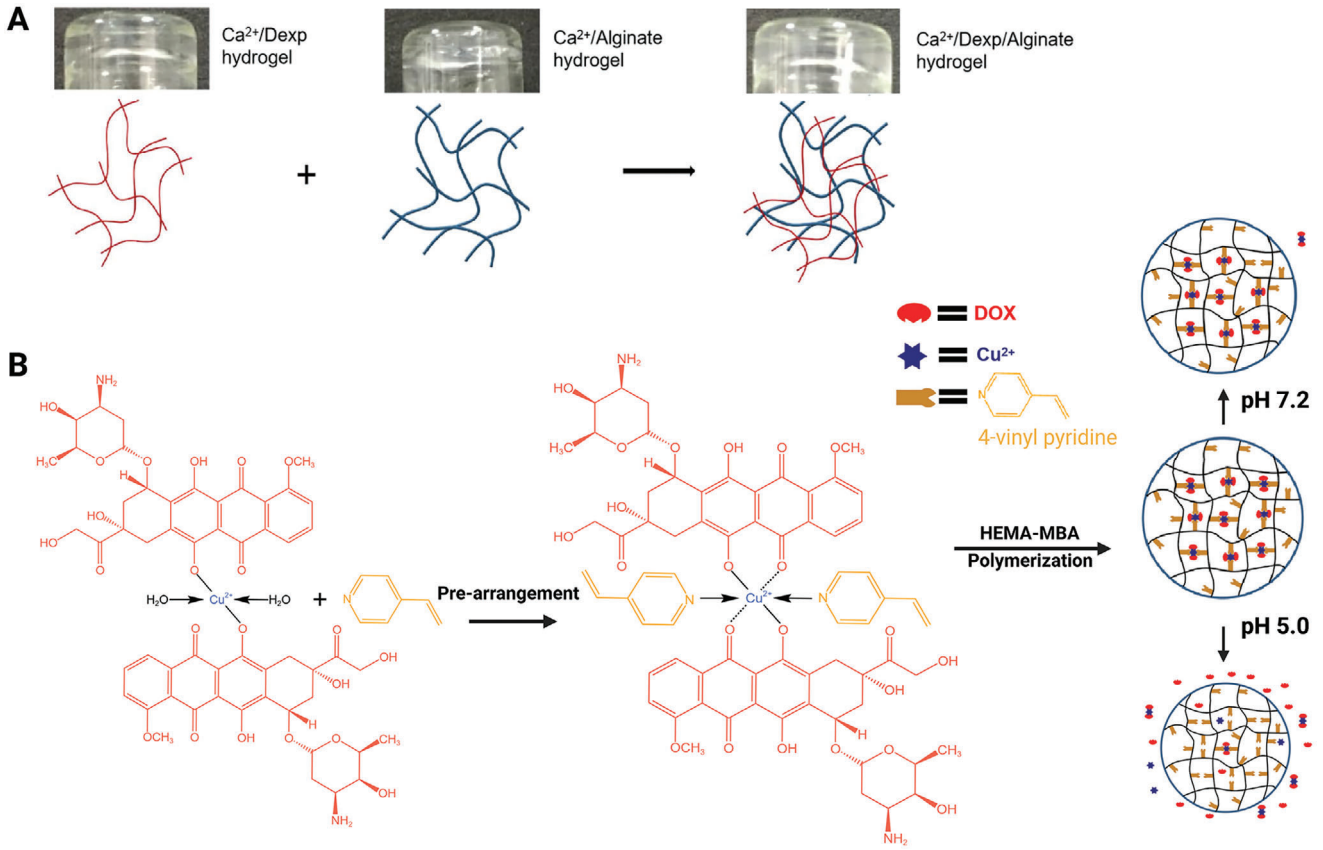

Figure 11. A) A scheme of hybrid hydrogel composition achieved through the combination of two different hydrogels: Ca^{2+}/DexP and Ca^{2+}/Alginate hydrogels. Adapted with permission.[133] Copyright 2019, Elsevier. B) Schematic mechanism of coordinated Dox imprinting and Dox release from the hydrogel. Adapted with permission.[35] Copyright 2021, Elsevier.

For example, these cargoes are relatively rigid, especially in the form of double-stranded nucleic acids, which carry negative charges, making penetrating the cell membrane and entering the cell difficult.[134] Another challenge is that nucleic acids are easily affected by various enzymes, especially nucleic acid hydrolases (such as DNase and RNase). Under normal physiological conditions, these enzymes quickly hydrolyze extracellular or abnormal enzymes, presenting a challenge that must be addressed as a drug for nucleic acids. The final issue lies in that the molecular weight of nucleic acid cargos in hydrogels ranges from thousands (siRNA) to millions (plasmid DNA) Daltons. Hence, nucleic acid cargo is extremely sensitive to external factors and is difficult to deliver to the target site, which is also the major obstacle to its clinical transformation.[135]

5.2.1. Metal Coordination DNA Hydrogel

DNA hydrogels can obtain a variety of stimulus responsiveness and controllable mechanical properties by rationally designing DNA sequences.[136] The abundant functional groups in DNA enable the hydrogels to conduct more reactions, thus promoting the application of DNA hydrogels. Certain metal ions are easy to readily coordinate with the base or phosphate group on the DNA, thus forming crosslinks into hydrogels. For example, Ag^+ could bind to cytosine (C) to compose C-Ag^+-C. Guo et al.[137] designed an Ag^+ crosslinked reversible DNA hydrogel. Because cysteine can form a more stable complex with Ag^+ than C-Ag^+, Ag^+ can be dissociated from the hydrogel after adding cysteine, making the hydrogel change from the gel state to the sol state (**Figure** 12A,B). SEM photograph (Figure 12C) shows that the hydrogel has a porous network structure. This strategy not only released DNA in specific regions to achieve targeted release but also prevented the DNA from being hydrolyzed by the enzymes during delivery. The generation of these hydrogels primarily relies on the coordination of Ag^+ with C and the π–π stacking interaction of the base within the system.

The Yang group used RCA to synthesize very long DNA strands containing multiple functional units including a DNAzyme sequence, a HhaI restriction site, and a recognition sequence for Cas9/sgRNA for (Figure 12D).[138] The DNA was assembled by Mn^{2+} ions to form NPs and then poly-glycerol dimethacrylate-(an acid-degradable polymer) with HhaI enzyme coating was loaded on the NPs to form a hybrid hydrogel. Inside acidic lysosomes, the polymer coating was disrupted, and the enzyme was responsible for DNA cleavage, releasing both Cas9/sgRNA and DNAzyme to inhibit gene expressions for efficient breast cancer therapy.

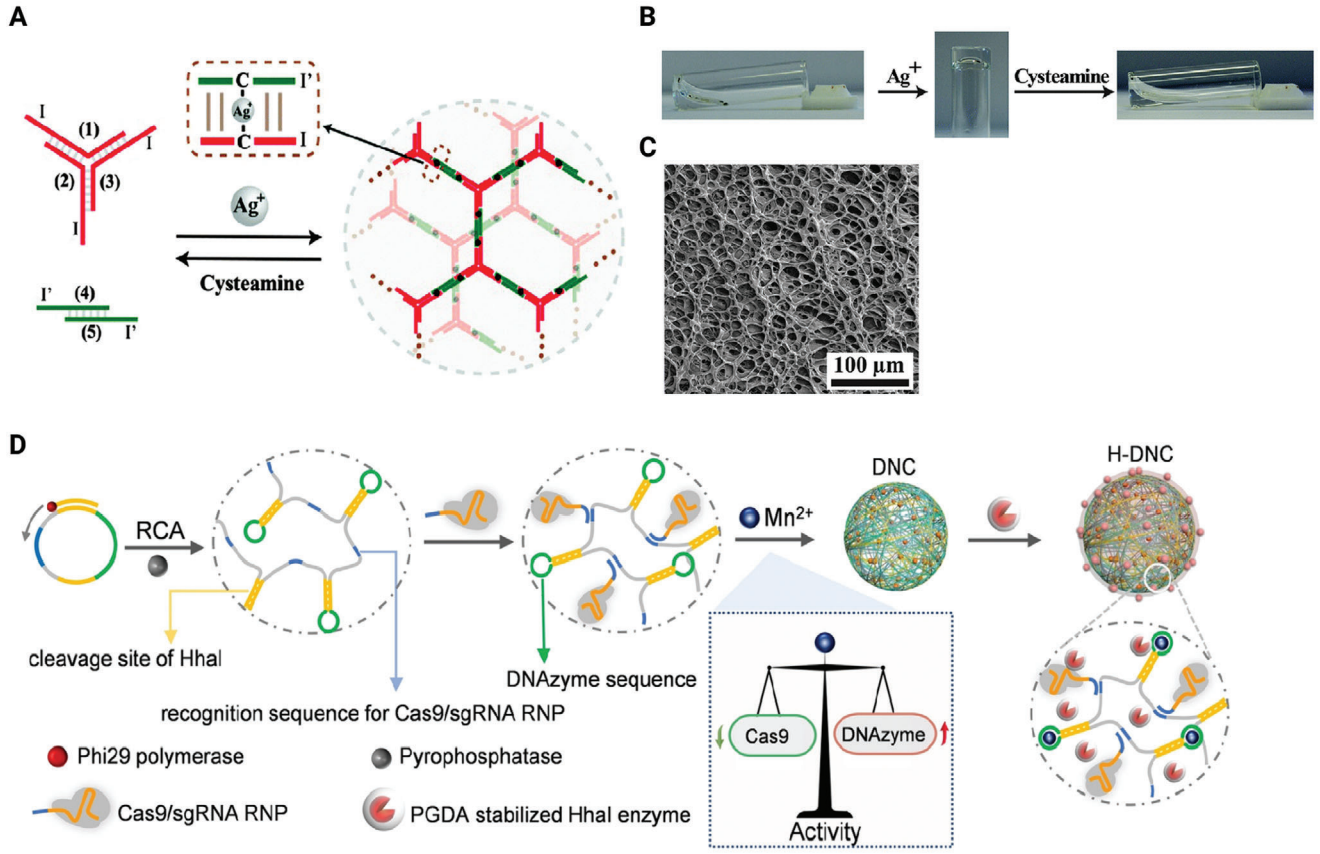

Figure 12. A) The assembly of a reversible DNA hydrogel induced by Ag^+. B) Images illustrating the cyclic transitions from solution to hydrogel and back to solution in the acrylamide–acrydite nucleic acid system, triggered by the crosslinking between the chains and Ag^+ ions. The system is separated when cysteamine is introduced into the system. C) SEM image showing the crosslinking of acrylamide–acrydite nucleic acid hydrogel with freeze-dried Ag^+. Adapted with permission.[137] Copyright 2023, Royal Society of Chemistry. D) Mn^{2+}-mediated assembly of an RCA product with multiple functional units. Adapted with permission.[138] Copyright 2022, John Wiley & Sons Inc.

5.2.2. Metal Coordination RNA Hydrogels

Similar to DNA, RNA can also be directly encapsulated into hydrogels. Fathil et al.[139] combined silver ions with lactoferrin and dicer-derived (siRNA) using coordination bonds. This siRNA, produced by the ribonuclease Dicer, has the ability to facilitate gene silencing. The resulting complex was encapsulated in a gelatin gel for the treatment of wounds in diabetic foot conditions. Examples of hydrogels with therapeutic RNA and metal ions based on metal coordination bonds are currently rare. One concern is the potential cleavage of RNA by a high concentration of metal ions under ambient conditions. When heated, the resulting materials might be NPs instead of hydrogels.

5.3. Peptide and Protein Drugs

Therapeutic proteins and peptides have become an indispensable part of the biopharmaceutical industry, especially in the fields of malignant tumors, diabetes, rheumatic diseases, and infectious diseases.[140] However, two obstacles limit the widespread application of protein drugs. The first is the prohibitive cost of cold chain transportation and storage,[141] and the second is that protein and peptide drugs require frequent administration. For example, anticancer drugs need to be used approximately once a month, whereas peptide hormones, such as insulin need to be administered at least once a day. These obstacles provide hydrogels an appropriate opportunity to stabilize protein drugs during transportation and storage, and reduce the frequency of drug administration through slow, continuous release.[142] In general, proteins larger than 100 kDa can be designed as hydrogels, and their release can be controlled through the degradation and diffusion of hydrogels.[143] For example, Lee et al.[144] found that physically crosslinked injectable hydrogels could efficiently deliver Avastin. In the model of metastatic colon cancer mouse, compared with the traditional frequency (once a week for four weeks), a single hydrogel injection achieved similar efficacy, and the maximum blood concentration in the peripheral circulation decreased to a quarter, realizing sustained, continuous drug release.

5.3.1. Peptides

There exist extensive literature studies on triggering peptide assembly using metal ions, including the formation of

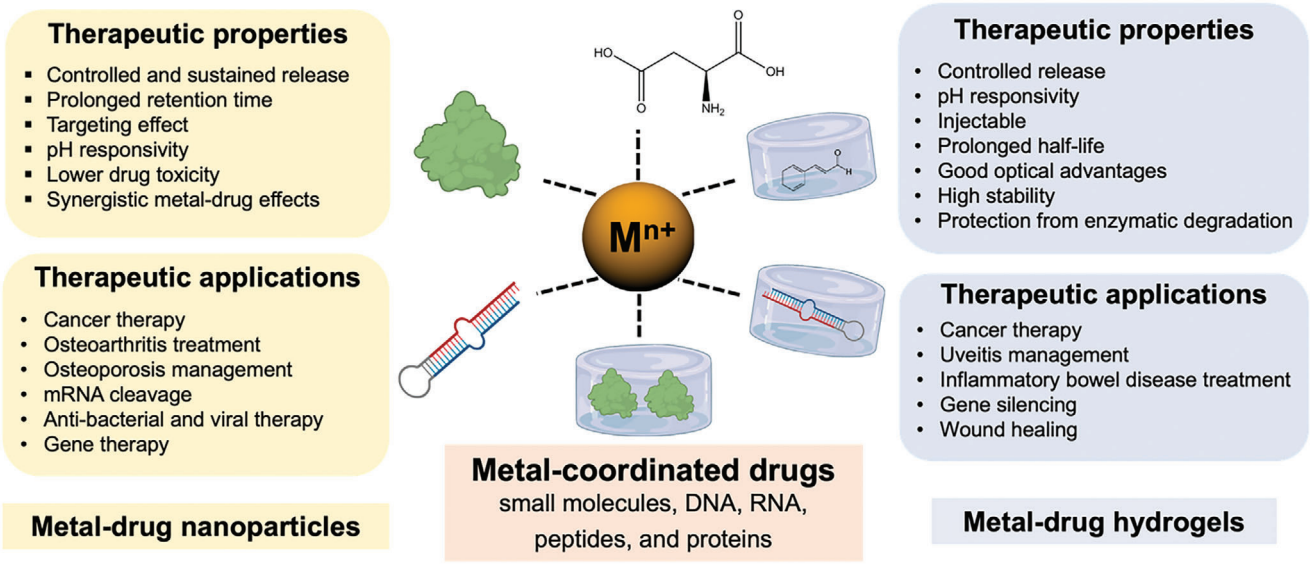

Figure 13. Summarizing the therapeutic properties and applications of metal–drug nanoparticles and hydrogels incorporating proteins, nucleic acids, or small molecules.

hydrogels,[145] although the examples of using therapeutic peptides for metal coordination are still limited. One such example is Bicalutamide, a drug for treating prostate cancer. He et al.[146] linked bicalutamide to a histidine hexapeptide (ID-1) that can self-assemble to form hydrogels with Zn^{2+} ions by using the effective coordination between Zn^{2+} and histidine. The authors injected the ID-1 drug conjugate into the prostate, an organ rich in Zn^{2+}, to enable in situ formation of hydrogels, which allowed for controlled release. The release of drug in this hydrogel demonstrated a tunable release profile in a typical acidic tumor microenvironment with esterase activity. As a result, this hydrogel demonstrated enhanced and selective cytotoxicity for killing prostate cancer cells.

Huang et al.[147] demonstrated an artificial peptide h9e via the combination of two native sequences from an elastic segment of spider silk and a transmembrane segment of human muscle L-type calcium channel. Ca^{2+} hydrogel could be used as an adjuvant of H1N1 influenza vaccine and improve the immune reactivity of inactivated H1N1 virus antigen by 70% to ensure biological safety.

5.3.2. Proteins

BSA is one of the most commonly used proteins for preparing metal protein coordination hydrogels. For example, the local inflammation of inflammatory bowel disease (IBD) and intestinal microthrombosis form a malicious cycle, exacerbating the progression of IBD.[148] Hong et al.[149] designed a hydrogel, which was crosslinked with heparin (HEP, Figure 1J) and bovine serum albumin (BSA) through Ag^{+} to form a HEP-Ag-BSA hydrogel. The hydrogel can be directly injected into the intestine and then assembled into a hydrogel in situ to cover the nidus in the intestinal tissue. Due to the electrostatic effect, the retention time of the hydrogel in the inflammatory intestinal mucosa tissue was considerably longer than that in the normal intestinal mucosa tissue, and it could effectively inhibit the formation of inflammatory microthrombosis and reduce the risk of bleeding.

Jiang et al.[150] designed a photosensitive-metal-effector protein hydrogel for the targeted delivery of neural repair proteins. In this system, a modified CarHC photosensitive protein coordinated with Zn^{2+} to form a hydrogel. With the help of the vitamin B12-dependent photosensitive effect of CarHC, it released nerve repair factors after corresponding light stimulation in the target area, improving the survival rate of neurons, and promoting axon regeneration.

6. Conclusions and Future Perspectives

In this article, we reviewed metal-coordinated drugs as advanced hybrid materials in the forms of NPs and hydrogels for therapeutic applications as summarized in **Figure 13**. Metal-coordinated NPs can be directly used for intravenous drug delivery and targeting ligands can also be added to the surface for active targeting. By forming hydrogels that can be locally applied, and thanks to the reversible coordination bonds, such materials are promising novel drug formulations for slow, sustained, and smart release. The only extra component is a metal ion. If choosing wisely, the additional toxicity imposed by carriers is minimal and there could be additional benefit from metal ions. Using metal coordination allows a high drug loading and minimal use of metal ions. The drugs include small molecules, nucleic acids, and proteins. The disease demonstrated so far ranged from cancer, viral infection, bacterial infection inflammatory bowel disease, to bone diseases. As demonstrated in this work, the medical use of metal coordination hydrogels has immense potential, especially the use of the characteristics of metal ions to customize hydrogels to respond to specific environmental factors or stimuli (such as pH, enzymes, ROS, light, sound, and magnetism) before drug release.[151]

Many future research opportunities are available to push this technology to clinical use. The first aspect is fundamental chemistry and materials science research. For example, it remains unclear when mixing a drug molecule with a metal ion can lead to the formation of NPs or hydrogels. Rational understanding and fine control on the outcome can advance the design of materials for their intended applications. The DexP studies provided an interesting example, where Fe^{2+} and Ca^{2+} produced NPs and hydrogels,[33,38] respectively, although the synthesis conditions are at very different temperatures. Side-by-side studies of different metal ions and different conditions in the same lab can provide the needed information. In addition, better control of the synthesis to have more homogeneous NPs needs to be achieved. Metal coordination is a unique way of assembling materials and knowledge can be borrowed from MOF chemistry.

Second, it is important to expand the range of drug molecules. So far, the majority of work on small molecule drugs are listed in Figure 1. One possible avenue for expansion comes from traditional medicine and natural products,[152] since they are rich in metal coordination groups, like carboxyl group in phenolic acid or heterocyclic oxygen in flavonoids. In addition, chemical modifications can be made to artificially introduce metal ligands. A good example is the addition of a phosphate group to Dex to make DexP, where this phosphate group plays a critical role in metal coordination. In addition, coassembly of a few different types of drugs with synergistic therapeutic applications could be interesting and useful. It is also important to systematically compare the toxicity of metal-coordinated drugs with the adsorption of drugs into porous nanomaterials carriers.

Finally, from the medical standpoint, a series of challenges need to be addressed in the future, such as the unique location of some tumors with poor blood supply, and how coordination materials respond to a specific microenvironment. Many cancer patients suffer not only from malignant tumors but also from complications like hypertension, hyperlipidemia, diabetes, chronic kidney disease, and acid-base metabolic disorders which may alter the hemorheology. Although some coordination materials have successfully passed tests for histocompatibility and hemolysis, maintaining a stable structure, and delivering drugs to the target area remains a challenge. This issue could be resolved by wrapping them with a biocompatible membrane.[153] Another limitation is that most current studies have a single experimental object, often tumor cell lines and animal disease models. These models are difficult to simulate the complex environment of patients' bodies. Therefore, we expect to replace original cell models with organoid models, and in vivo models should gradually be replaced with induced in situ cancer models rather than transplanted tumor models to achieve better evaluation results. These issues highlight the importance of interdisciplinary work in this field, which will benefit from the in-depth collaboration between physicians, biologists, pharmaceutical chemists, and materials scientists.

Acknowledgements

K.-Y.W. and Z.N. contributed equally to this work. The authors thanked David Zia for proofreading the manuscript. Funding for this work was from the Hong Kong Special Administrative Region Government and InnoHK. They also thanked the support from the National Natural Science Foundation of China (No. 82274371), the Natural Science Foundation of Hunan Province (No. 2023JJ30944), and the Postdoctoral Fellowship Program of CPSF (No. GZC20233176).

Conflict of Interest

The authors declare no conflict of interest.

Keywords

DNA, drug delivery, hydrogels, metal coordination, nanomedicine

Received: March 19, 2024
Revised: April 8, 2024
Published online:

[1] Y. Zhong, F. Meng, C. Deng, Z. Zhong, *Biomacromolecules* **2014**, *15*, 1955.
[2] K. Swetha, N. G. Kotla, L. Tunki, A. Jayaraj, S. K. Bhargava, H. Hu, S. R. Bonam, R. Kurapati, *Vaccines* **2023**, *11*, 658.
[3] W. Chen, S. Zhou, L. Ge, W. Wu, X. Jiang, *Biomacromolecules* **2018**, *19*, 1732.
[4] V. De Matteis, *Toxics* **2017**, *5*, 29.
[5] C. L. Ventola, *P&T* **2017**, *42*, 742.
[6] Y. Huang, J. C. Hsu, H. Koo, D. P. Cormode, *Theranostics* **2022**, *12*, 796.
[7] R. A. Alsahafi, H. A. Mitwalli, A. A. Balhaddad, M. D. Weir, H. H. K. Xu, M. A. S. Melo, *Front. Dent. Med.* **2021**, *2*, 743065.
[8] Z. Liu, L. Xie, K. Qiu, X. Liao, T. W. Rees, Z. Zhao, L. Ji, H. Chao, *ACS Appl. Mater. Interfaces* **2020**, *12*, 31205.
[9] a) M.-X. Wu, Y.-W. Yang, *Adv. Mater.* **2017**, *29*, 1606134; b) J. Yang, Y.-W. Yang, *Small* **2020**, *16*, 1906846.
[10] a) Y. Liu, Z. Tang, *Chemistry* **2012**, *18*, 1030; b) J. Zhou, H. Han, J. Liu, *Nano Res.* **2021**, *15*, 71.
[11] S. Wang, M. Wahiduzzaman, L. Davis, A. Tissot, W. Shepard, J. Marrot, C. Martineau-Corcos, D. Hamdane, G. Maurin, S. Devautour-Vinot, C. Serre, *Nat. Commun.* **2018**, *9*, 4937.
[12] a) W. Rieter, K. Pott, K. Taylor, W. Lin, *J. Am. Chem. Soc.* **2008**, *130*, 11584; b) W. Lin, W. Rieter, K. Taylor, *Angew. Chem.* **2009**, *48*, 650; c) G. Palermo, A. Spinello, A. Saha, A. Magistrato, *Expert Opin. Drug Dis.* **2021**, *16*, 497.
[13] a) Y. Ding, Z. Tong, L. Jin, B. Ye, J. Zhou, Z. Sun, H. Yang, L. Hong, F. Huang, W. Wang, Z. Mao, *Adv. Mater.* **2022**, *34*, 2106388; b) G. Yu, S. Yu, M. L. Saha, J. Zhou, T. R. Cook, B. C. Yung, J. Chen, Z. Mao, F. Zhang, Z. Zhou, Y. Liu, L. Shao, S. Wang, C. Gao, F. Huang, P. J. Stang, X. Chen, *Nat. Commun.* **2018**, *9*, 4335; c) K. Yang, S. Qi, X. Yu, B. Bai, X. Zhang, Z. Mao, F. Huang, G. Yu, *Angew. Chem.* **2022**, *61*, e202203786.
[14] a) D.-L. Ma, C. Wu, S.-S. Cheng, F.-W. Lee, Q.-B. Han, C.-H. Leung, *Int. J. Mol. Sci.* **2019**, *20*, 341; b) I. Amarsy, S. Papot, G. Gasser, *Angew. Chem.* **2022**, *61*, e202205900; c) M. Huynh, R. Vinck, B. Gibert, G. Gasser, *Adv. Mater.* **2024**, *1*, 2311437.
[15] a) Y. Liu, S. Lv, D. Liu, F. Song, *Acta Biomater.* **2020**, *116*, 16; b) P. Štarha, R. Křikavová, *Coord. Chem. Rev.* **2024**, *501*, 215578; c) H. Geng, Q.-Z. Zhong, J. Li, Z. Lin, J. Cui, F. Caruso, J. Hao, *Chem. Rev.* **2022**, *122*, 11432.
[16] H. Zhang, L. Kang, Q. Zou, X. Xin, X. Yan, *Curr. Opin. Biotechnol.* **2019**, *58*, 45.
[17] C. He, D. Liu, W. Lin, *Chem. Rev.* **2015**, *115*, 11079.
[18] T. Cook, V. Vajpayee, M. Lee, P. Stang, K. Chi, *Acc. Chem. Res.* **2013**, *46*, 2464.

[19] a) T. Tomohiro, Y. Ogawa, H. Okuno, M. Kodaka, *J. Am. Chem. Soc.* **2003**, *125*, 14733; b) T. Wadas, E. Wong, G. Weisman, C. Anderson, *Chem. Rev.* **2010**, *110*, 2858.
[20] A. K. Renfrew, *Metallomics* **2014**, *6*, 1324.
[21] M. D. Rowe, D. H. Thamm, S. L. Kraft, S. G. Boyes, *Biomacromolecules* **2009**, *10*, 983.
[22] J. Xu, J. Wang, J. Ye, J. Jiao, Z. Liu, C. Zhao, B. Li, Y. Fu, *Adv. Sci.* **2021**, *8*, e2101101.
[23] a) A. Xu, P. Yang, C. Yang, Y. Gao, X. Zhao, Q. Luo, X. Li, L. Li, L. Wang, H. Wang, *Nanoscale* **2016**, *8*, 14078; b) Y. Yang, W. Zhu, L. Feng, Y. Chao, X. Yi, Z. Dong, K. Yang, W. Tan, Z. Liu, M. Chen, *Nano Lett.* **2018**, *18*, 6867.
[24] a) J. Kim, H. Cho, H. Jeon, D. Kim, C. Song, N. Lee, S. Choi, T. Hyeon, *J. Am. Chem. Soc.* **2017**, *139*, 10992; b) Z. Tang, Y. Liu, M. He, W. Bu, *Angew. Chem.* **2019**, *58*, 946.
[25] T. R. Cook, Y.-R. Zheng, P. J. Stang, *Chem. Rev.* **2013**, *113*, 734.
[26] M. Wu, J. Yang, T. Ye, B. Wang, Y. Tang, X. Ying, *ACS Appl. Mater. Interfaces* **2023**, *15*, 29939.
[27] J. Das, Y. J. Choi, J. W. Han, A. Reza, J. H. Kim, *Sci. Rep.* **2017**, *7*, 9513.
[28] C. Ge, Y. Li, J.-J. Yin, Y. Liu, L. Wang, Y. Zhao, C. Chen, *NPG Asia Mater.* **2012**, *4*, e32.
[29] L. Tu, Z. Fan, F. Zhu, Q. Zhang, S. Zeng, Z. Chen, L. Ren, Z. Hou, S. Ye, Y. Li, *J. Mater. Chem. B* **2020**, *8*, 5667.
[30] H. Geng, M. Zhou, B. Li, L. Liu, X. Yang, Y. Wen, H. Yu, H. Wang, J. Chen, L. Chen, *Chem. Eng. J.* **2021**, *417*, 128103.
[31] S. Liang, M. Wang, J. Wang, G. Chen, *ChemBioChem* **2021**, *22*, 3184.
[32] L. Ruan, M. Wang, M. Zhou, H. Lu, J. Zhang, J. Gao, J. Chen, Y. Hu, *ACS Appl. Bio. Mater.* **2019**, *2*, 4703.
[33] L. Tang, Z. Di, J. Zhang, F. Yin, L. Li, L. Zheng, *Nano Res.* **2023**, *16*, 13259.
[34] H. Dong, X. Hong, Y. He, Z. Bao, Y. Zhang, S. Shen, G. Wang, J. Zhang, R. Mo, *Biomater. Sci.* **2022**, *10*, 4356.
[35] Q. Zhang, L. Zhang, P. Wang, S. Du, *J. Pharm. Sci.* **2014**, *103*, 643.
[36] P. Yavvari, S. Pal, S. Kumar, A. Kar, A. Awasthi, A. Naaz, A. Srivastava, A. Bajaj, *ACS Biomater. Sci. Eng.* **2017**, *3*, 3404.
[37] W. Pi, L. Wu, J. Lu, X. Lin, X. Huang, Z. Wang, Z. Yuan, H. Qiu, J. Zhang, H. Lei, P. Wang, *Bioact. Mater.* **2023**, *29*, 98.
[38] W. Wu, Z. Zhang, T. Xiong, W. Zhao, R. Jiang, H. Chen, X. Li, *Acta Biomater.* **2017**, *61*, 157.
[39] Y. Wu, Z. Yang, X. Li, T. Li, J. Zheng, M. Hu, Z. Yu, W. Luo, W. Zhang, F. Zheng, T. Tang, Y. Wang, *Chem. Eng. J.* **2023**, *477*, 147145.
[40] J. Bi, Y. Lu, Y. Dong, P. Gao, *J. Nanomater.* **2018**, *2018*, 1357812.
[41] J. Zhao, Y. Zhu, C. Ye, Y. Chen, S. Wang, D. Zou, Z. Li, *Int. J. Nanomed.* **2019**, *14*, 3893.
[42] Z. Ma, B. Moulton, *Coord. Chem. Rev.* **2011**, *255*, 1623.
[43] B. Morak-Młodawska, M. Jeleń, E. Martula, R. Korlacki, *Int. J. Mol. Sci.* **2023**, *24*, 6970.
[44] J. K. Patra, G. Das, L. F. Fraceto, E. V. R. Campos, M. d. P. Rodriguez-Torres, L. S. Acosta-Torres, L. A. Diaz-Torres, R. Grillo, M. K. Swamy, S. Sharma, S. Habtemariam, H.-S. Shin, *J. Nanobiotechnol.* **2018**, *16*, 71.
[45] S. Onoue, S. Yamada, H. K. Chan, *Int. J. Nanomed.* **2014**, *9*, 1025.
[46] R. Kumar, P. F. Siril, S. V. Dalvi, *ACS Appl. Nano Mater.* **2020**, *3*, 4944.
[47] G. C. M'bitsi-Ibouily, T. Marimuthu, P. Kumar, Y. E. Choonara, L. C. du Toit, P. Pradeep, G. Modi, V. Pillay, *Sci. Rep.* **2019**, *9*, 4146.
[48] K. Wosikowski, L. Lamphere, G. Unteregger, V. Jung, F. Kaplan, J. Xu, B. Rattel, M. Caligiuri, *Cancer Chemother. Pharmacol.* **2007**, *60*, 589.
[49] a) J. Dobbs, D. Shin, S. Krishnamurthy, H. Kuerer, W. Yang, R. Richards-Kortum, *Int. J. Cardiol.* **2016**, *139*, 1140; b) L. Ireland, A. Santos, M. Ahmed, C. Rainer, S. Nielsen, V. Quaranta, U. Weyer-Czernilofsky, D. Engle, P. Perez-Mancera, S. Coupland, A. Taktak, T. Bogenrieder, D. Tuveson, F. Campbell, M. Schmid, A. Mielgo, *Cancer Res.* **2016**, *76*, 6851.
[50] J. Mazumdar, V. Dondeti, M. Simon, *J. Cell. Mol. Med.* **2009**, *13*, 4319.
[51] H. Maeda, H. Nakamura, J. Fang, *Adv. Drug Delivery Rev.* **2013**, *65*, 71.
[52] J. Nagy, H. Dvorak, *Clin. Exp. Metastasis* **2012**, *29*, 657.
[53] D. Gilkes, G. Semenza, D. Wirtz, *Nat. Rev. Cancer* **2014**, *14*, 430.
[54] M. Takasawa, R. Moustafa, J. Baron, *Stroke* **2008**, *39*, 1629.
[55] M. Watson, P. Vignali, S. Mullett, A. Overacre-Delgoffe, R. Peralta, S. Grebinoski, A. Menk, N. Rittenhouse, K. DePeaux, R. Whetstone, D. Vignali, T. Hand, A. Poholek, B. Morrison, J. Rothstein, S. Wendell, G. Delgoffe, *Nature* **2021**, *591*, 645.
[56] Y. Dai, C. Xu, X. Sun, X. Chen, *Chem. Soc. Rev.* **2017**, *46*, 3830.
[57] Q. Gao, J. Feng, W. Liu, C. Wen, Y. Wu, Q. Liao, L. Zou, X. Sui, T. Xie, J. Zhang, Y. Hu, *Adv. Drug Delivery Rev.* **2022**, *188*, 114445.
[58] X. Yang, Q. Tang, Y. Jiang, M. Zhang, M. Wang, L. Mao, *J. Am. Chem. Soc.* **2019**, *141*, 3782.
[59] R. S. Johan, H. Valma, J. Asko, K. Juha, F. Carol, G. Per-Henrik, L. Markku, *BMJ Open Diabetes Res. Care* **2015**, *3*, e000067.
[60] Q. Tang, L. Shi, B. Yang, W. Liu, B. Li, Y. Jin, *J. Mater. Chem. B* **2023**, *11*, 3413.
[61] L. Nan, C. Liu, H. Song, X. Wang, P. Wang, L. Fang, *Int. J. Pharm.* **2024**, *649*, 123575.
[62] S. Gautam, I. Lakhanpal, L. Sonowal, N. Goyal, *Next Nanotechnol.* **2023**, *3–4*, 100027.
[63] X. Liu, Z. Chen, J. Bai, X. Li, X. Chen, Z. Li, H. Pan, S. Li, Q. Gao, N. Zhao, A. Chen, H. Xu, Y. Wen, L. Du, M. Yang, X. Zhou, J. Huang, *ACS Nano* **2023**, *17*, 25377.
[64] H. Tian, S. Zhao, E. Nice, C. Huang, W. He, B. Zou, J. Lin, *J. Colloid Interface Sci.* **2022**, *607*, 1516.
[65] a) J. Munawar, M. S. Khan, S. E. Zehra Syeda, S. Nawaz, F. A. Janjhi, H. Ul Haq, E. U. Rashid, T. Jesionowski, M. Bilal, *Inorg. Chem. Commun.* **2023**, *147*, 110145; b) V. Chandrakala, V. Aruna, G. Angajala, *Emergent Mater.* **2022**, *5*, 1593.
[66] a) M. Z. Alyami, S. K. Alsaiari, Y. Li, S. S. Qutub, F. A. Aleisa, R. Sougrat, J. S. Merzaban, N. M. Khashab, *J. Am. Chem. Soc.* **2020**, *142*, 1715; b) Y. Zhang, X. Zhang, H. Li, J. Liu, W. Wei, J. Gao, *Membranes* **2022**, *12*, 738.
[67] a) C. H. Evans, V. B. Kraus, L. A. Setton, *Nat. Rev. Rheumatol.* **2014**, *10*, 11; b) J. Gao, Z. Xia, H. B. Mary, J. Joseph, J. N. Luo, N. Joshi, *Trends Pharmacol. Sci.* **2022**, *43*, 171.
[68] a) P. Cacoub, T. Asselah, *Am. J. Gastroenterol.* **2022**, *117*, 253; b) P. H. Almeida, C. E. L. Matielo, L. A. Curvelo, R. A. Rocco, G. Felga, B. D. Guardia, Y. L. Boteon, *World J. Gastroenterol.* **2021**, *27*, 3249.
[69] C. Bode, G. Zhao, F. Steinhagen, T. Kinjo, D. M. Klinman, *Expert Rev. Vaccines* **2011**, *10*, 499.
[70] X. Gao, Y. Liu, W. Huo, Y. Song, Y. Chen, J. Zhang, X. Yang, Y. Jin, X.-j. Liang, *Nanoscale* **2023**, *15*, 11346.
[71] N. H. Khan, A. A. Bui, Y. Xiao, R. B. Sutton, R. W. Shaw, B. J. Wylie, M. P. Latham, *PLoS One* **2019**, *14*, e0214440.
[72] J. A. Kulkarni, D. Witzigmann, S. B. Thomson, S. Chen, B. R. Leavitt, P. R. Cullis, R. van der Meel, *Nat. Nanotechnol.* **2021**, *16*, 630.
[73] B. Liu, J. Zhang, L. Li, *Chemistry* **2019**, *25*, 13452.
[74] M. Li, C. Wang, Z. Di, H. Li, J. Zhang, W. Xue, M. Zhao, K. Zhang, Y. Zhao, L. Li, *Angew. Chem.* **2019**, *58*, 1350.
[75] a) S. S. Athavale, A. S. Petrov, C. Hsiao, D. Watkins, L. D. Williams, *PLoS One* **2012**, *7*, e38024; b) W. J. Moon, J. Liu, *ChemBioChem* **2020**, *21*, 401.
[76] D. M. Klinman, *Nat. Rev. Immunol.* **2004**, *4*, 249.
[77] L. Zhang, L. Zhang, Y. Wang, K. Jiang, C. Gao, P. Zhang, Y. Xie, B. Wang, Y. Zhao, H. Xiao, J. Song, *Nano Res.* **2023**, *5*, 4758.
[78] Y. Wang, L. Zhang, Y. Liu, L. Tang, J. He, X. Sun, M. Younis, D. Cui, H. Xiao, D. Gao, X. Kong, W. Cai, J. Song, *Adv. Healthcare Mater.* **2022**, *11*, e2201178.

[79] P. Ji, X. Deng, X. Jin, S. Zhang, J. Wang, J. Feng, W. Chen, X. Zhang, *Adv. Healthcare Mater.* **2023**, *12*, e2300323.
[80] S. Li, S. Jiang, M. Rahman, J. Mei, X. Wang, J. Jiang, Y. Chen, S. Xu, Y. Liu, *Small Methods* **2023**, *7*, e2201569.
[81] X. Liu, F. Li, Z. Dong, C. Gu, D. Mao, J. Chen, L. Luo, Y. Huang, J. Xiao, Z. Li, Z. Liu, Y. Yang, *Sci. Adv.* **2023**, *9*, eadf3329.
[82] B. Liu, F. Hu, J. Zhang, C. Wang, L. Li, *Angew. Chem.* **2019**, *58*, 8804.
[83] C. Liu, Y. Chen, J. Zhao, Y. Wang, Y. Shao, Z. Gu, L. Li, Y. Zhao, *Angew. Chem.* **2021**, *60*, 14324.
[84] Q. Zhang, S. Yu, J. Shang, S. He, X. Liu, F. Wang, *Small* **2023**, *20*, e2305672.
[85] X. Feng, B. Liu, Z. Zhou, W. Li, J. Zhao, L. Li, Y. Zhao, *Nano Res.* **2023**, *16*, 12633.
[86] C. Wang, Z. Di, Z. Fan, L. Li, *Chem. Res. Chin. U J.* **2020**, *36*, 6.
[87] a) W. Zhou, R. Saran, J. Liu, *Chem. Rev.* **2017**, *117*, 8272; b) L. Li, H. Xing, J. Zhang, Y. Lu, *Acc. Chem. Res.* **2019**, *52*, 2415.
[88] a) S. Santoro, G. Joyce, *Proc. Natl. Acad. Sci. USA* **1997**, *94*, 4262; b) W. Zhou, J. Ding, J. Liu, *Theranostics* **2017**, *7*, 1010.
[89] a) H. Fan, Z. Zhao, G. Yan, X. Zhang, C. Yang, H. Meng, Z. Chen, H. Liu, W. Tan, *Angew. Chem.* **2015**, *54*, 4801; b) H. Wang, Y. Chen, H. Wang, X. Liu, X. Zhou, F. Wang, *Angew. Chem.* **2019**, *58*, 7380; c) J. Wei, H. Wang, Q. Wu, X. Gong, K. Ma, X. Liu, F. Wang, *Angew. Chem.* **2020**, *59*, 5965.
[90] J. Yu, Y. Zhang, L. Li, Y. Xiang, X. Yao, Y. Zhao, K. Cai, M. Li, Z. Li, Z. Luo, *Acta Biomater.* **2023**, *169*, 434.
[91] H. Gu, K. Furukawa, Z. Weinberg, D. Berenson, R. Breaker, *J. Am. Chem. Soc.* **2013**, *135*, 9121.
[92] Z. Du, L. Zhu, P. Wang, X. Lan, S. Lin, W. Xu, *Small* **2023**, *19*, e2301048.
[93] K. Jiang, Y. Chen, D. Zhao, J. Cheng, F. Mo, B. Ji, C. Gao, C. Zhang, J. Song, *Nanoscale* **2020**, *12*, 18682.
[94] R. Zhong, S. Talebian, B. Mendes, G. Wallace, R. Langer, J. Conde, J. Shi, *Nat. Mater.* **2023**, *22*, 818.
[95] U. Sahin, K. Karikó, Ö. Türeci, *Nat. Rev. Drug Discovery* **2014**, *13*, 759.
[96] B. Davidson, P. McCray, *Nat. Rev. Genet.* **2011**, *12*, 329.
[97] J. Finn, A. Smith, M. Patel, L. Shaw, M. Youniss, J. van Heteren, T. Dirstine, C. Ciullo, R. Lescarbeau, J. Seitzer, R. Shah, A. Shah, D. Ling, J. Growe, M. Pink, E. Rohde, K. Wood, W. Salomon, W. Harrington, C. Dombrowski, W. Strapps, Y. Chang, D. Morrissey, *Cell Rep.* **2018**, *22*, 2227.
[98] K. Paunovska, D. Loughrey, J. Dahlman, *Nat. Rev. Genet.* **2022**, *23*, 265.
[99] S. Ku, S. Jo, Y. Lee, K. Kim, S. Kim, *Adv. Drug Delivery Rev.* **2016**, *104*, 16.
[100] J. Kulkarni, D. Witzigmann, S. Chen, P. Cullis, R. van der Meel, *Acc. Chem. Res.* **2019**, *52*, 2435.
[101] a) L. Wang, J. Sloand, A. Gaffey, C. Venkataraman, Z. Wang, A. Trubelja, D. Hammer, P. Atluri, J. Burdick, *Biomacromolecules* **2017**, *18*, 77; b) M. Vázquez-González, I. Willner, *Angew. Chem.* **2020**, *59*, 15342.
[102] Z. Zou, L. He, X. Deng, H. Wang, Z. Huang, Q. Xue, Z. Qing, Y. Lei, R. Yang, J. Liu, *Angew. Chem.* **2021**, *60*, 22970.
[103] Y. Liu, X. Wang, H. Chen, T. Wu, Y. Cao, Z. Liu, *ACS Appl. Mater. Interfaces* **2023**, *15*, 8937.
[104] S. Huang, H. Le, G. Hong, G. Chen, F. Zhang, L. Lu, X. Zhang, Y. Qiu, Z. Wang, Q. Zhang, G. Ouyang, J. Shen, *Acta Biomater.* **2022**, *148*, 244.
[105] Z. Huang, B. Liu, J. Liu, *ChemComm* **2020**, *56*, 4208.
[106] a) C. Mirkin, S. Petrosko, *Nat. Nanotechnol.* **2018**, *13*, 624; b) R. Merindol, S. Loescher, A. Samanta, A. Walther, *Nat. Nanotechnol.* **2018**, *13*, 730.
[107] C. Lu, Y. Xu, P. Huang, M. Zandieh, Y. Wang, J. Zheng, J. Liu, *Nanoscale* **2022**, *14*, 14613.
[108] Q. Han, X. Zhang, Y. Jia, S. Guo, J. Zhu, S. Luo, N. Na, J. Ouyang, *Chemistry* **2022**, *28*, e202200281.
[109] B. Buntz, *Drug Dicovery Develop.* **2023**. https://www.drugdiscoverytrends.com/best-selling-pharmaceuticals-2023/.
[110] a) X. Ma, H. Fei, *Prog. Chem.* **2016**, *28*, 184; b) N. Yoshinari, N. Kuwamura, T. Kojima, T. Konno, *Coord. Chem. Rev.* **2023**, *474*, 214857.
[111] M. Kai, S. Wang, W. Gao, L. Zhang, *J. Cardiopulm. Rehabil.* **2023**, *361*, 178.
[112] C. Wang, Z. Di, Z. Xiang, J. Zhao, L. Li, *Nano Today* **2021**, *38*, 101140.
[113] H. Sun, R. Chang, Q. Zou, R. Xing, W. Qi, X. Yan, *Small* **2019**, *15*, 1905326.
[114] E. Argitekin, E. Ersoz-Gulseven, G. Cakan-Akdogan, Y. Akdogan, *Biomacromolecules* **2023**, *24*, 3603.
[115] Y. Akdogan, S. Cigdem Sozer, C. Akyol, M. Basol, C. Karakoyun, G. Cakan-Akdogan, *J. Mol. Liq.* **2022**, *367*, 120575.
[116] E. Ahmed, *J. Adv. Res.* **2015**, *6*, 105.
[117] T. McMahon, K. Zadnik, *Cornea* **2000**, *19*, 730.
[118] W. Li, G. Cheng, S. Wang, Y. Jiang, X. Liu, Q. Huang, *Int. J. Biol. Macromol.* **2024**, *260*, 129398.
[119] N. Ninan, A. Forget, V. Shastri, N. Voelcker, A. Blencowe, *ACS Appl. Mater. Interfaces* **2016**, *8*, 28511.
[120] W. Zheng, L. Wang, H. Jiao, Z. Wu, Q. Zhao, T. Lin, H. Ma, Z. Zhang, X. Xu, J. Cao, J. Zhong, J. Xu, B. Lu, *Chem. Eng. J.* **2023**, *455*, 140553.
[121] a) S. Kim, S. Kwon, S. Jeon, E. Yu, S. Park, *Int. J. Cosmet. Sci.* **2014**, *36*, 553; b) J. Sun, X. Xie, Y. Song, T. Sun, X. Liu, H. Yuan, C. Shen, *Bioact. Mater.* **2024**, *35*, 495; c) S. Aswathy, U. Narendrakumar, I. Manjubala, *Heliyon* **2020**, *6*, e03719.
[122] F. Vernerey, S. Lalitha Sridhar, A. Muralidharan, S. Bryant, *Chem. Rev.* **2021**, *121*, 11085.
[123] a) T. Shao, N. Falcone, H. Kraatz, *ACS Omega* **2020**, *5*, 1312; b) J. Haitjema, L. Wu, A. Giuliani, L. Nahon, S. Castellanos, A. Brouwer, *Phys. Chem. Chem. Phys.* **2021**, *23*, 20909.
[124] N. Burtch, H. Jasuja, K. Walton, *Chem. Rev.* **2014**, *114*, 10575.
[125] A. Tsiouris, A. Mayer, J. Wiltink, C. Ruckes, M. Beutel, R. Zwerenz, *JMIR Cancer* **2023**, *9*, e42123.
[126] W. Quan, Z. Hu, H. Liu, Q. Ouyang, D. Zhang, S. Li, P. Li, Z. Yang, *Molecules* **2019**, *24*, 2586.
[127] L. Shi, P. Ding, Y. Wang, Y. Zhang, D. Ossipov, J. Hilborn, *Macromol. Rapid Commun.* **2019**, *40*, e1800837.
[128] a) H. Li, P. Yang, P. Pageni, C. Tang, *Macromol. Rapid Commun.* **2017**, *38*, 1700109; b) W. Sun, B. Xue, Q. Fan, R. Tao, C. Wang, X. Wang, Y. Li, M. Qin, W. Wang, B. Chen, Y. Cao, *Sci. Adv.* **2020**, *6*, eaaz9531.
[129] W. Yuan, Z. Li, X. Xie, Z. Zhang, L. Bian, *Bioact. Mater.* **2020**, *5*, 819.
[130] R. Binaymotlagh, L. Chronopoulou, F. Haghighi, I. Fratoddi, C. Palocci, *Materials* **2022**, *15*, 5871.
[131] J. Neumann, S. Lee, E. Zhao, P. Fenter, *ChemPhysChem* **2023**, *24*, 202300742.
[132] a) D. Dang, K. Riaz, D. Karamichos, *Drugs* **2022**, *82*, 145; b) A. Lee, H. Blair, *Drugs* **2020**, *80*, 1101.
[133] R. Zhang, L. Lei, Q. Song, X. Li, *Colloids Surf., B* **2019**, *175*, 569.
[134] a) D. Gary, N. Puri, Y. Won, *J. Cardiopulm. Rehabil.* **2007**, *121*, 64; b) S. Hendrikse, S. Gras, A. Ellis, *ACS Nano* **2019**, *13*, 8512.
[135] S. Correa, A. Grosskopf, H. L. Hernandez, D. Chan, A. Yu, L. Stapleton, E. Appel, *Chem. Rev.* **2021**, *121*, 11385.
[136] a) C. Li, A. Faulkner-Jones, A. Dun, J. Jin, P. Chen, Y. Xing, Z. Yang, Z. Li, W. Shu, D. Liu, R. Duncan, *Angew. Chem.* **2015**, *54*, 3957; b) X. Mao, G. Chen, Z. Wang, Y. Zhang, X. Zhu, G. Li, *Chem. Sci.* **2018**, *9*, 811.
[137] W. Guo, X. Qi, R. Orbach, C. Lu, L. Freage, I. Mironi-Harpaz, D. Seliktar, H. Yang, I. Willner, *ChemComm* **2014**, *50*, 4065.
[138] F. Li, N. Song, Y. Dong, S. Li, L. Li, Y. Liu, Z. Li, D. Yang, *Angew. Chem.* **2022**, *61*, e202116569.
[139] M. Fathil, H. Katas, *Pharm* **2023**, *15*, 991.

[140] L. Urquhart, *Nat. Rev. Drug Discovery* **2018**, *17*, 232.
[141] R. Welch, H. Lee, M. Luzuriaga, O. Brohlin, J. Gassensmith, *Bioconjug. Chem.* **2018**, *29*, 2867.
[142] C. Meis, E. Salzman, C. Maikawa, A. Smith, J. Mann, A. Grosskopf, E. Appel, *ACS Biomater. Sci. Eng.* **2021**, *7*, 4221.
[143] A. Bertz, S. Wöhl-Bruhn, S. Miethe, B. Tiersch, J. Koetz, M. Hust, H. Bunjes, H. Menzel, *J. Bioprocess. Biotech.* **2013**, *163*, 243.
[144] A. Lee, V. Ng, S. Gao, J. Hedrick, Y. Yang, *Biomacromolecules* **2015**, *16*, 465.
[145] R. Zou, Q. Wang, J. Wu, J. Wu, C. Schmuck, H. Tian, *Chem. Soc. Rev.* **2015**, *44*, 5200.
[146] S. He, L. Mei, C. Wu, M. Tao, Z. Zhai, K. Xu, W. Zhong, *Nanoscale* **2019**, *11*, 5030.
[147] H. Huang, J. Shi, J. Laskin, Z. Liu, D. S. Mcvey, X. S. Sun, *Soft Matter* **2011**, *7*, 8905.
[148] T. Li, C. Wang, Y. Liu, B. Li, W. Zhang, L. Wang, M. Yu, X. Zhao, J. Du, J. Zhang, Z. Dong, T. Jiang, R. Xie, R. Ma, S. Fang, J. Zhou, J. Shi, *J. Crohns. Colitis* **2020**, *14*, 240.
[149] L. Hong, G. Chen, Z. Cai, H. Liu, C. Zhang, F. Wang, Z. Xiao, J. Zhong, L. Wang, Z. Wang, W. Cui, *Adv. Sci.* **2022**, *9*, e2200281.
[150] B. Jiang, X. Liu, C. Yang, Z. Yang, J. Luo, S. Kou, K. Liu, F. Sun, *Sci. Adv.* **2020**, *6*, eabc4824.
[151] G. Dai, L. Sun, J. Xu, G. Zhao, Z. Tan, C. Wang, X. Sun, K. Xu, W. Zhong, *Acta Biomater.* **2021**, *129*, 84.
[152] a) M. S. Wong, C. C. Poon, L. P. Zhou, H. H. Xiao, *Handb. Exp. Pharmacol.* **2020**, *262*, 499; b) N. Kumar, N. Goel, *Biotechnol. Rep.* **2019**, *24*, e00370.
[153] R. H. Fang, W. Gao, L. Zhang, *Nat. Rev. Clin. Oncol.* **2023**, *20*, 33.

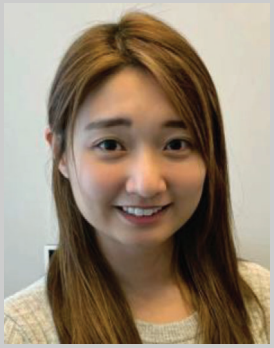

Ka-Ying Wong received her Ph.D. in Applied Biology and Chemical Technology from The Hong Kong Polytechnic in 2020. She is currently a postdoctoral fellow in Prof. Juewen Liu's lab in the Department of Chemistry at the University of Waterloo. Her present research focuses on drug discovery and delivery through the application of aptamers and nanotechnology.

Zhenyu Nie received his M.D. degrees at Central South University in 2023. Since 2023, he has joined the Xiangya Hospital, Central South University. Currently, he is a research associate and postdoctoral fellow of Central South University. His research interests include bladder cancer, drug delivery, and hydrogel.

Man-sau Wong received her Ph.D. degree in Human Nutrition and Nutritional Biology at the University of Chicago. She is currently the Director of the Research Center for Chinese Medicine Innovation and Professor at the Department of Food Science and Nutrition at the Hong Kong Polytechnic University. She is a Certified Food Scientist and Registered Nutritionist. Her research interests include Chinese medicine and musculoskeletal health; molecular actions of bone protective phytochemicals and phytoestrogens, the role of gut microbiota in mediating the therapeutic actions of Chinese herbs, as well as Chinese medicine-based drug discovery and delivery for vision health.

Yang Wang received his B.Sc. and Ph.D. degrees at Central South University in 2010 and 2016, respectively. Since 2016, he has joined the Xiangya Hospital, Central South University. Currently, he is a professor in Xiangya Hospital, Central South University. His research interests include Chinese medicine-based drug delivery, self-assembling biomaterials, and nanomedicine.

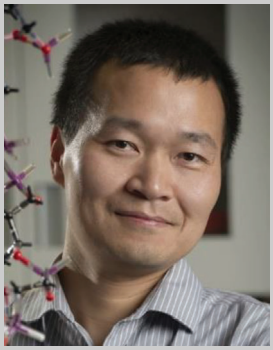

Juewen Liu received his Ph.D. degree from the University of Illinois at Urbana-Champaign in 2005. He is currently a professor of chemistry at the University of Waterloo, and a College member of the Royal Society of Canada (RSC). He serves as a Section Editor for Biosensors & Bioelectronics, and a Contributing Editor for Trends in Analytical Chemistry. He is interested in metal-dependent DNAzymes, aptamers, biointerface sciences, and nanozymes. He has published over 400 papers, receiving over 40 000 citations with an H-index of 102. He is a Highly Cited Researcher listed by Clarivate in 2022 and 2023.